Electronic Supplementary Material (ESI) for Inorganic Chemistry Frontiers.

Copper catalysts for photo- and electro-catalytic hydrogen production

Abdullah M. Abudayyeh,[1] Olivier Schott,[2] Humphrey L. C. Feltham,[a] Garry S. Hanan[2] and Sally Brooker[1]**

[1]Department of Chemistry and MacDiarmid Institute for Advanced Materials and Nanotechnology, University of Otago, PO Box 56, Dunedin 9054, New Zealand.
E-mail: sbrooker@chemistry.otago.ac.nz

[2]Département de Chimie, Université de Montréal, Quebec, Canada.

Electronic Supporting Information

Contents

1. Photocatalytic HER

1.1 General protocol

Reagents and solutions: $[Ru(bpy)_3](PF_6)_2$ (bpy = 2,2'-bipyridine) was first used as the photosensitizer (PS) in cobalt catalysed hydrogen evolution reactions (HER) by Sauvage in 1979[1] and Lehn in 1982,[2] and remains the most commonly used PS in the literature, so is also employed herein. Based on our previous report on 17 cobalt complexes active for HER under photocatalytic conditions,[3] using dimethylformamide (99.9 % ACS grade, DMF) as solvent, triethanolamine (TEOA) as sacrificial electron donor, HBF_4 or water as proton sources, and blue 10 W LED irradiation (445 nm; 88 $mW.cm^{-2}$), these too have been used herein.

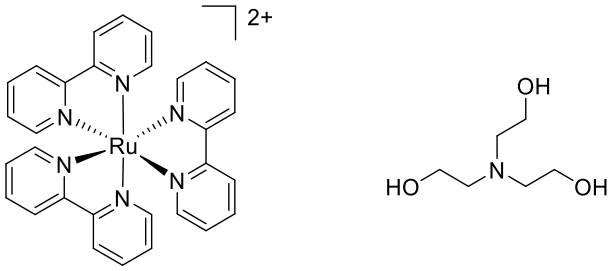

$[Ru(bpy)_3]^{2+}$ TEOA

Figure S1. Photosensitizer and sacrificial electron donor (TEOA) employed in this work.

All photocatalytic HER tests were carried out at the University of Montreal by either AA or OS. Before each experiment, new solutions were prepared :

1) 2 M triethanolamine (TEOA) as sacrificial donor plus 0.2 M HBF_4 from 48 wt.% aqueous HBF_4 so associated with that is 1.06 M water, as proton sources, along with some protons from the photo-oxidation of TEOA.[4]
2) 0.8 mM photosensitizer $[Ru(bpy)_3](PF_6)_2$
3) 20 µM copper catalyst

For each test, 2.5 mL of the sacrificial electron donor/proton source stock solution (solution 1), 1.25 mL of the photosensitizer stock solution (solution 2) and 1.25 mL of the catalyst stock solution (solution 3) were added to a standard 20 mL glass vial. The molar concentrations of the components in the resulting 5 mL reaction solution were as follows:

Sacrificial donor: 1.0 M TEOA

Proton source: 0.1 M HBF_4 and 0.53 M water

Photosensitizer: 0.2 mM $[Ru(bpy)_3](PF_6)_2$

Catalyst: 5 µM copper(II) complex or simple salt

The resulting apparent pH was recorded as being between 8.7 and 8.9 for all initial photocatalytic solutions, using a SB20 pH-meter calibrated as usual in aqueous buffer. But it must be noted that in organic media (here DMF) the proton activity at the interface of the electrode is different, so the reading is an 'apparent' pH. Nevertheless this simple approach was used in 1983 by the pioneers of the development of molecular photocatalytic systems for hydrogen generation, who employed cobaloxime and macrocyclic cobalt complexes.[5]

Gas chromatography (GC) analysis: The vial containing the 5 mL of reaction solution was promptly placed in a 20°C thermostated photoreactor that can be illuminated by a blue 10 W LED set at the desired irradiation power (88 $mW.cm^{-2}$). An analog power-meter PM100A (THORLABS) associated with a compact photodiode power head with silicon detector S120C is used to evaluate the power of the photon flux. Photo-diode detector is placed at the same distance from the LED surface than the bottom of illuminated vial. The vials are continuously stirred and bubbled in a controlled way by use of Mass Flow Controllers (Alicat 0-20 SCCM) which are set to deliver a stable flow rate of argon of 10 mL/min. The vial is sealed with a rubber septum pierced by two stainless-steel cannulae. The upstream stainless-steel cannula joins a pre-loaded vial containing 5 mL of dry DMF (to saturate the gas with solvent before it enters the reaction vial). The downstream stainless-steel cannula connects to a 2 mL empty vial (to protect the GC from any accidental droplet of DMF) which is connected to an 8-port stream select valve (VICCI). The selected valve allows the gas stream from the reaction vial to fill the sample loop of the GC. A digital flowmeter (Perkin Elmer FlowMark) is used to check the flow. The solutions are degassed for 30 min under argon flow before turning on the light. A microprocessor (Arduino Uno) coupled with a custom PC interface controls the intervals (defined times) at which gas injections are taken from the reaction vial into the GC sample loop.

The photocatalysis gas samples are analysed using a PerkinElmer Clarus-480 gas chromatograph (GC). The instrument is equipped with a thermal conductivity detector (TCD) for the quantification of hydrogen, a 7 inch HayeSep N 60/80 pre-column and a 9 inch molecular sieve 13*45/60 column for the separation of gas and a 2 mL injection loop. Argon is the carrier and eluent gas.

A calibration curve, to establish the relationship (equation 1) between the integration of the H_2 signal in the TCD trace (y) and the concentration of H_2 in the gas sample (x), is determined by flowing different, accurately known, concentrations of standard H_2 gas mixtures (balance of mixture is argon) into the sample loop and integrating the observed area under the H_2 peak in the TCD trace.

$$y = ax + b \qquad \text{eq (1)}$$

x = concentration of H_2, in $\mu L.L^{-1}$ (known for calibration, but to be determined for the catalysts later)
y = H_2 TCD area, in µV.s
a = slope
b = noise of H_2 TCD area without hydrogen present, in µV.s

Calibration establishes the values of *a* (the constant of proportionality, or slope) and *b* (noise correction) in equation 1. With these values in hand, when a catalyst is tested the area of the observed H_2 peak in the TCD trace can be converted, using equation 1, into the concentration of H_2 in $\mu L.L^{-1}$ ($\mu L_{H2}.L^{-1}$). The flow rate of the argon vector gas is known, so the rate of H_2 generation can be readily calculated using equation 2:

$$\text{Rate of production of } H_2 \ (\mu L_{H2}.min^{-1}) = [H_2 \text{ standard}] \ (\mu L_{H2}.L^{-1}) \times \text{Ar flow rate } (L.min^{-1}) \qquad \text{(eq 2)}$$

The ideal gas law (eq 3) then permits the conversion of volume of H_2 in L to the amount of substance in mol :

$$PV = nRT \quad \leftrightarrow \quad n = PV/RT \qquad \text{(eq 3)}$$

P = pressure = 1 atm
T = temperature = 298 K
R = ideal gas constant = 0.082 $L.atm.K^{-1}.mol^{-1}$
V = volume of hydrogen in L
n = amount of hydrogen in mol

1.2 Control experiments

1.2.1 Dark reaction blanks for catalysts 1-3

In each experiment, monitoring of the head gas by GC for 20-40 min before switching the blue LED light on (dark experiment) showed that, as expected, no hydrogen was observed (Figure S2-S**4**).

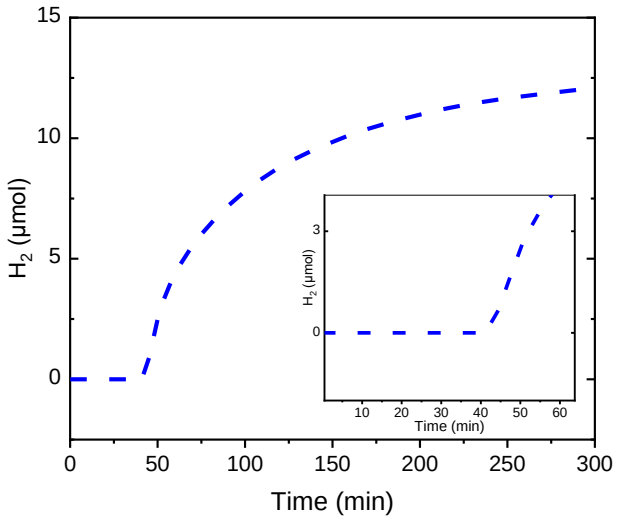

Figure S2. Hydrogen generation profile of **1** (5 µM) in DMF at 20 °C, with 1.0 M TEOA, 0.2 mM $[Ru(bpy)_3](PF_6)_2$, 0.1 M HBF_4 and 0.53 M of water – for 40 mins in the dark (control confirms no hydrogen forms in the dark; expansion shown in the inset) before turning on irradiation with a blue LED (λ = 445 nm, 88 mW/cm^2).

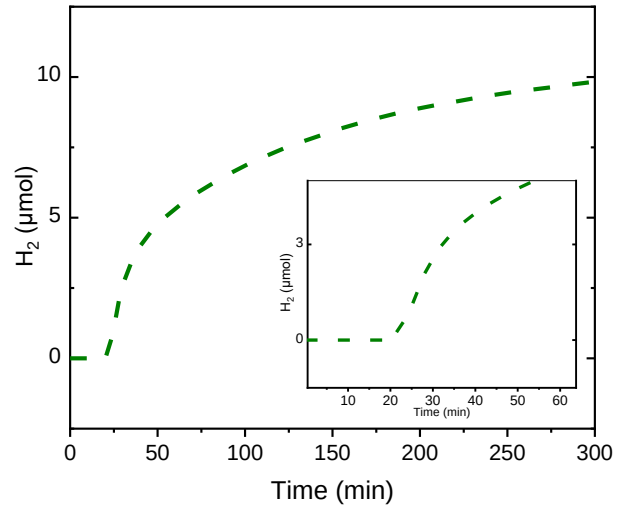

Figure S3. Hydrogen generation profile of **2** (5 µM) in DMF at 20 °C, with 1.0 M TEOA, 0.2 mM $[Ru(bpy)_3](PF_6)_2$, 0.1 M HBF_4 and 0.53 M of water - for 20 minutes mins in the dark (control confirms no hydrogen forms in the dark; expansion shown in the inset) before turning on irradiation with a blue LED (λ = 445 nm, 88 mW/cm^2).

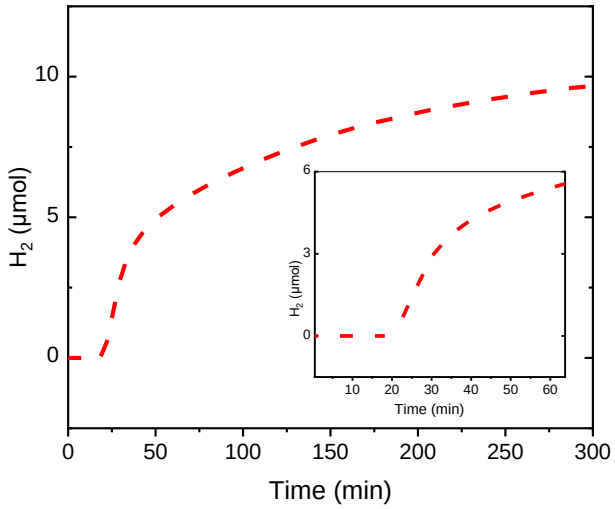

Figure S4. Hydrogen generation profile of **3** (5 µM) in DMF at 20 °C, with 1.0 M TEOA, 0.2 mM $[Ru(bpy)_3](PF_6)_2$ 0.1 M HBF_4 and 0.53 M of water - for 20 minutes in the dark (control confirms no hydrogen forms in the dark; expansion shown in the inset) before turning on irradiation with a blue LED (λ = 445 nm, 88 mW/cm^2).

1.2.2 No PS blank

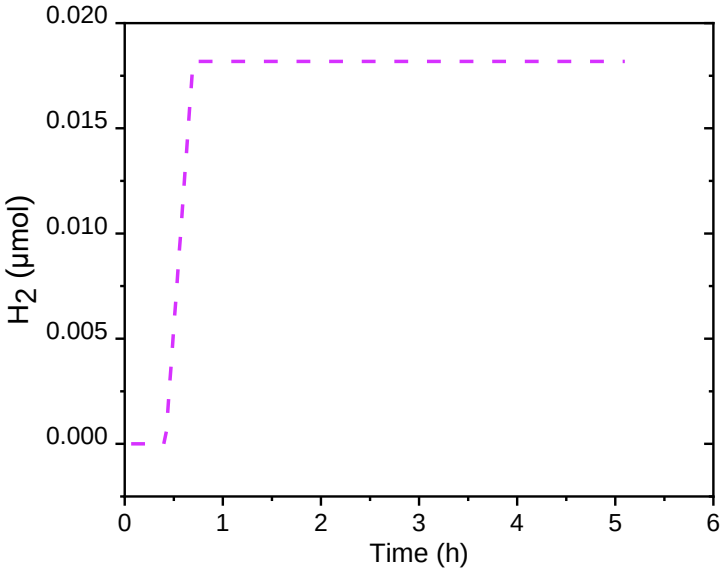

Figure S5. Hydrogen evolution-time profile for **1** (5 µM) in DMF in the absence of photosensitizer under irradiation with a blue LED (λ = 445 nm, 88 mW/cm^2) at 20 °C, with 1.0 M TEOA, and 0.1 M HBF_4 and 0.53 M of water. Negligible amount of hydrogen produced, 0.018 µmol, compared with more than ≥ 10 µmol produced when all components present (see Figures S2-S4).

1.2.3 No copper catalyst blank

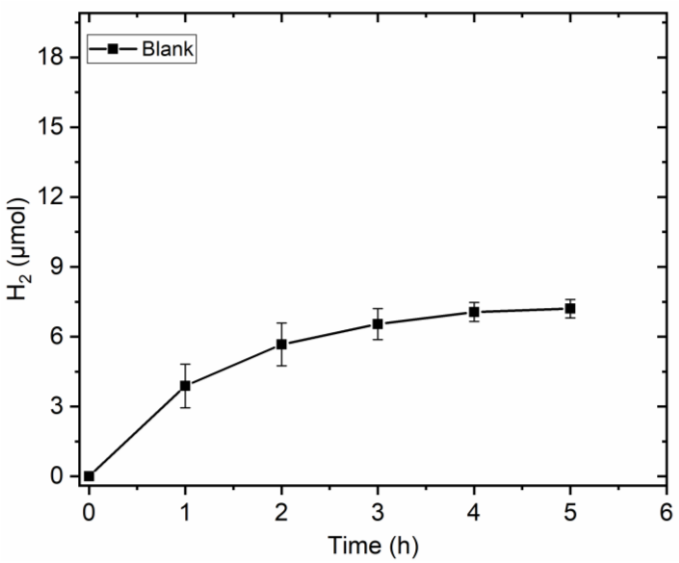

Figure S6. Hydrogen evolution-time profile for blank experiment averaged of multiple runs (4 runs), irradiation of DMF solution with a blue LED (λ = 445 nm, 88 mW/cm^2) at 20 °C, with 1.0 M TEOA, 0.2 mM $[Ru(bpy)_3](PF_6)_2$, 0.1 M HBF_4 and 0.53 M of water.

1.2.4. Control with simple copper salts as catalyst:

$Cu(BF_4)_2.xH_2O$ and $Cu(NO_3)_2.3H_2O$

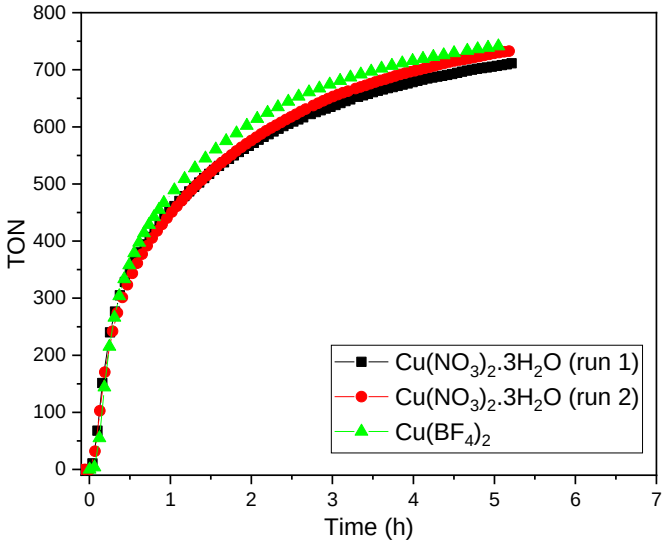

Figure S7. Hydrogen evolution-time profile for control experiments with 5 µM of simple copper(II) salts in DMF: (black and red) $Cu(NO_3)_2.3H_2O$ and (green) $Cu(BF_4)_2.xH_2O$, upon irradiation with a blue LED (λ = 445 nm, 88 mW/cm^2) at 20 °C, with 1.0 M TEOA, 0.2 mM $[Ru(bpy)_3](PF_6)_2$, 0.1 M HBF_4 and 0.53 M of water.

1.3 Plot of TOFs for 1-3 and half life calculations

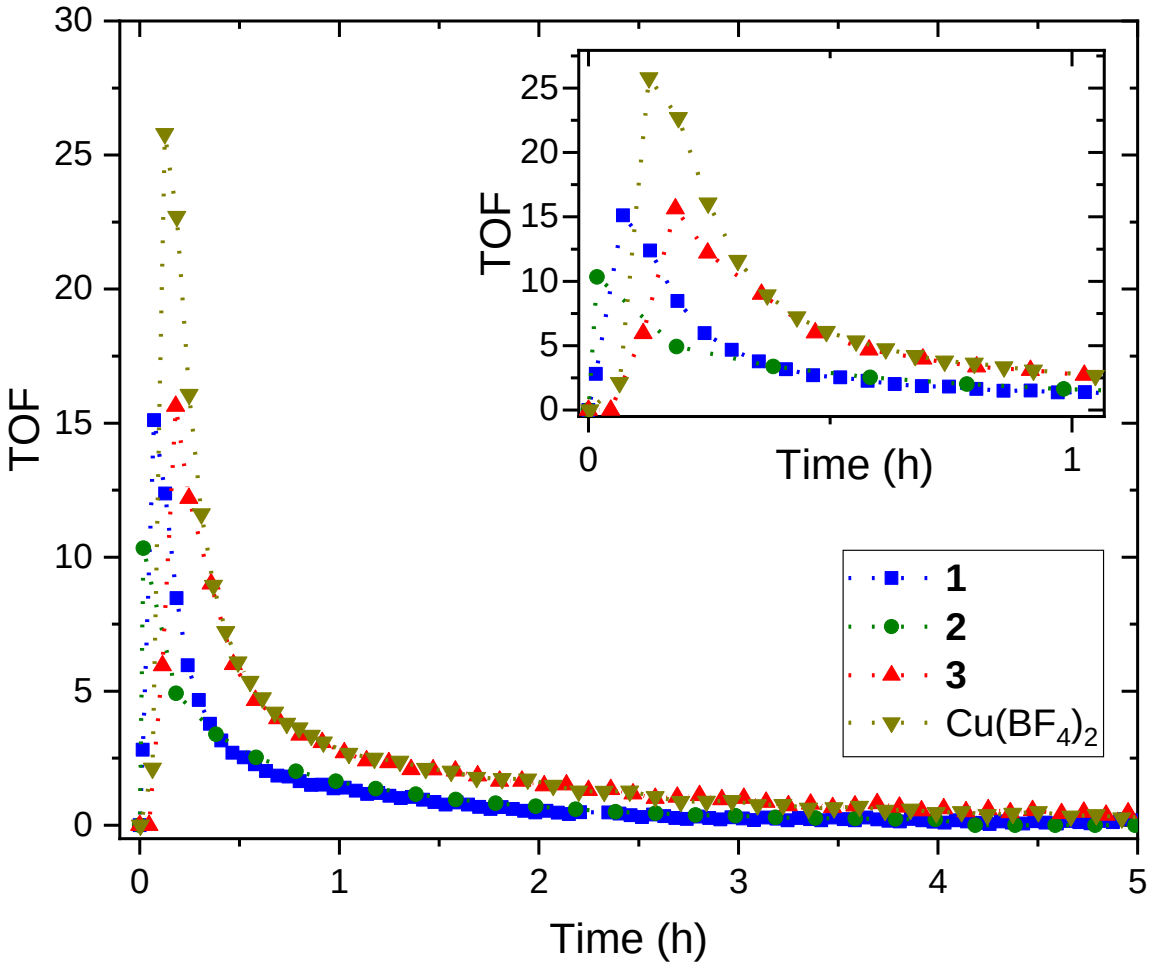

Figure S8. Turnover frequency (TOF: mol H_2/mol cat/ min) vs time profile, for copper complexes **1** [Cu^{II} **L**^{Et}]BF_4 (blue), **2** [Cu^{II} **L**$^{Et\text{-}MePy}$]BF_4 (green), **3** [Cu^{II} **L**^{EtPy2}]BF_4 (red), as well as for the 'control' $Cu^{II}(BF_4)_2$ (dark yellow), in DMF, with $C_{cat.}$ = 5 µM, upon irradiation with a blue LED (λ = 445 nm, 88 mW/cm^2) at 20 °C, with 1.0 M TEOA, 0.2 mM $[Ru(bpy)_3](PF_6)_2$, 0.1 M HBF_4 and 0.53 M of water. The inset shows an expansion of the TOFs over the first hour.

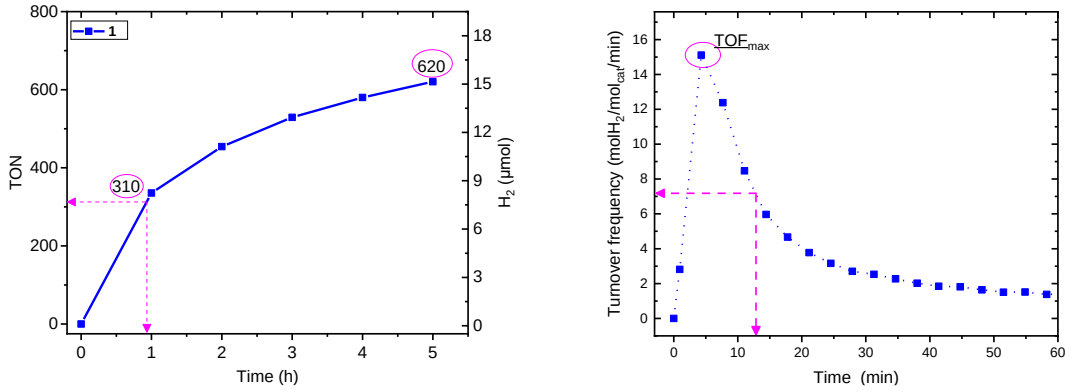

Figure S9. (Left) Turnover number (TON) and (right) turnover frequency (TOF/ min^{-1}) vs time profile, for copper complexes **1** $[Cu^{II}\,\mathbf{L}^{Et}]BF_4$ showing the HER progress, (magenta line) (left) the time taken for the catalyst to reach half of its maximum turnover $t_{1/2}$ 56 min., (right) the time taken for this activity to drop by 50%, $t_{1/2}$ 13 min.

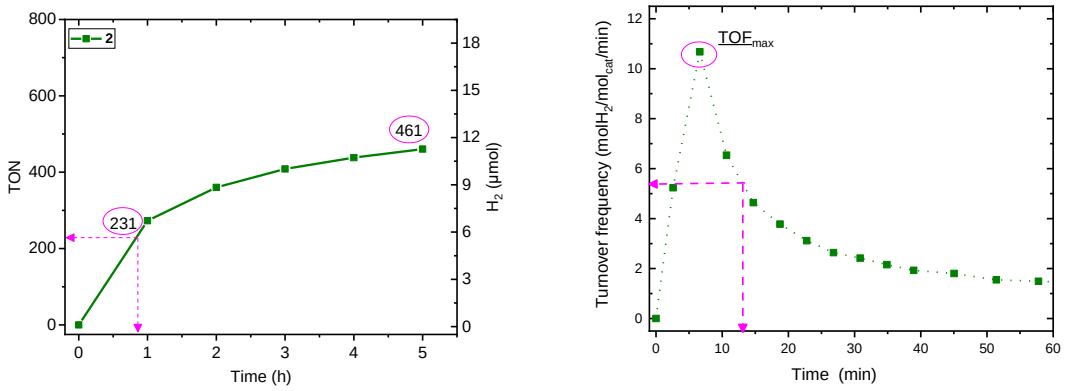

Figure S10. (Left) Turnover number (TON) and (right) turnover frequency (TOF/ min^{-1}) vs time profile, for copper complexes **2** $[Cu^{II}\,\mathbf{L}^{Et\text{-}MePy}]BF_4$ showing the HER progress, (magenta line) (left) the time taken for the catalyst to reach half of its maximum turnover $t_{1/2}$ 52 min., (right) the time taken for this activity to drop by 50%, $t_{1/2}$ 13 min.

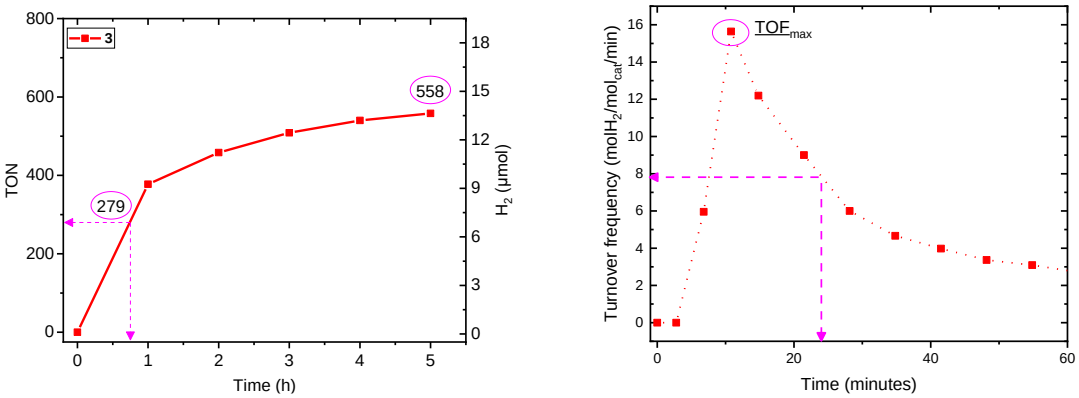

Figure S11. (Left) Turnover number (TON) and (right) turnover frequency (TOF/ min^{-1}) vs time profile, for copper complexes **3** $[Cu^{II}\,\mathbf{L}^{EtPy2}]BF_4$ showing the HER progress, (magenta line) (left) the time taken for the catalyst to reach half of its maximum turnover $t_{1/2}$ 44 min., (right) the time taken for this activity to drop by 50%, $t_{1/2}$ 24 min.

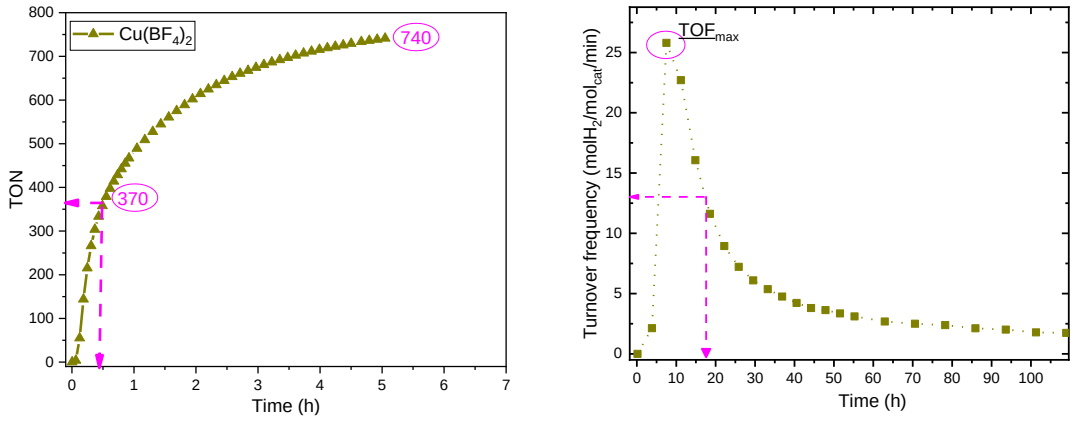

Figure 12. (Left) Turnover number (TON) and (right) turnover frequency (TOF/ min^{-1}) vs time profile, for copper complexes **3** $[Cu^{II}\,\mathbf{L}^{EtPy2}]BF_4$ showing the HER progress, (magenta line) (left) the time taken for the salt to reach half of its maximum turnover $t_{1/2}$ 28 min., (right) the time taken for this activity to drop by 50%, $t_{1/2}$ 17 min.

1.4 Additional plots and tables

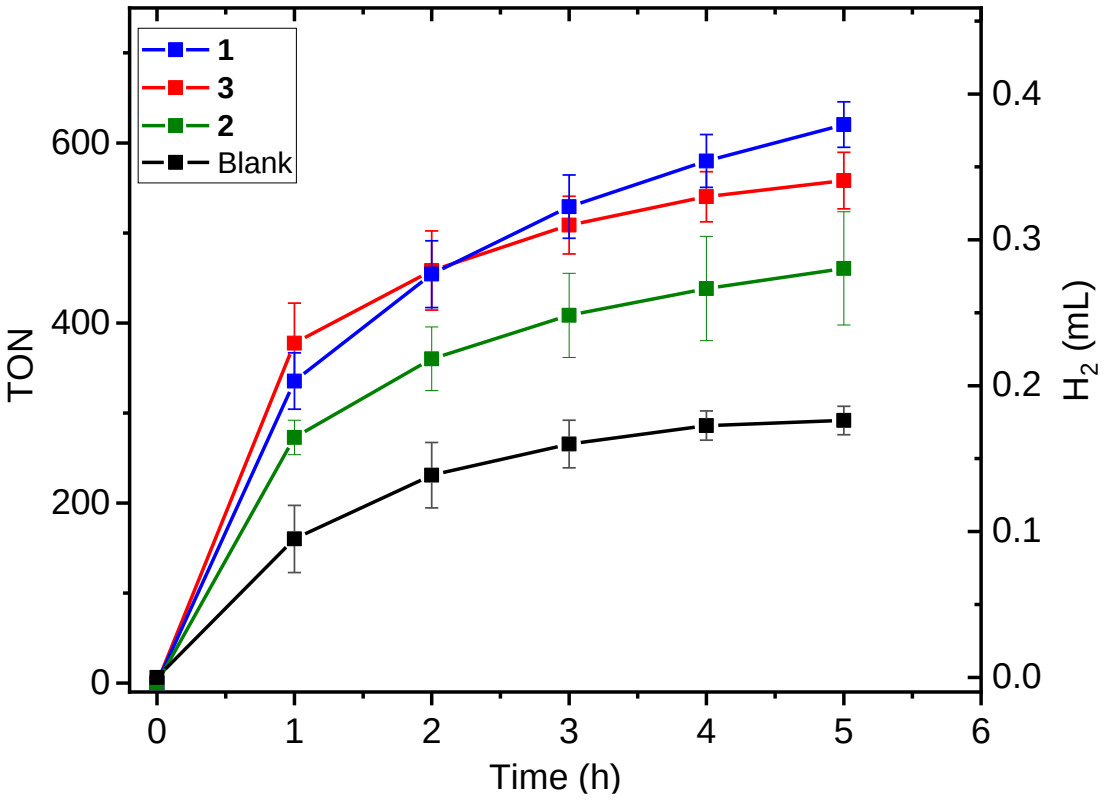

Figure S13. Hydrogen evolution (mL) vs time profile for copper complexes **1** $[Cu^{II}\,\mathbf{L}^{Et}]BF_4$ (blue), **2** $[Cu^{II}\,\mathbf{L}^{Et\text{-}MePy}]BF_4$ (green), **3** $[Cu^{II}\,\mathbf{L}^{EtPy2}]BF_4$ (red), as well as for the 'blank' experiments (no catalyst) (black), in DMF ($C_{cat.}$ = 5 μM) upon irradiation with a blue LED (λ = 445 nm, 88 mW/cm^2) at 20 °C, with 1.0 M TEOA, 0.2 mM $[Ru(bpy)_3](PF_6)_2$, 0.1 M HBF_4 and 0.53 M of water.

Table S1. Consistency of HER performance of copper complexes **1**-**3** in DMF solution under photocatalytic conditions over multiple runs.[a] See also Figures S13-S15 below.

Catalyst	TON[b]						H_2 (μmol) [c]						TOF (min^{-1})					
	Run 1	Run 2	Run 3	Run 4	Run 5	**Average**	Run 1	Run 2	Run 3	Run 4	Run 5	**Average**	Run 1	Run 2	Run 3	Run 4	Run 5	**Average**
1	583	635	627	648	609	**620±25**	14.6	15.8	15.7	16.2	15.2	**15.5±0.6**	15.1	15.5	17.6	16.4	15.7	**16.1±1.0**
2	432	400	421	498	552	**461±63**	10.8	10.0	10.0	12.5	13.8	**11.4±1.7**	10.3	11.6	10.7	9.6	12.9	**11.0±1.3**
3·0.5H_2O	559	531	602	541		**558±31**	14.0	13.3	15.0	13.5		**14.0±0.7**	18.1	14.5	17.3	15.6		**16.4±1.6**
No copper							7.6	7.4	7.1	6.7		**7.2± 0.4**						
Control $Cu(BF_4)_2$	741						18.5						25.8					
Control $Cu(NO_3)_2$	707	730				**719±16**	17.6	18.2				**17.9±0.4**	25.7	21.2				**23.5±3.2**

[a] conditions: 6 h irradiation with a blue LED (λ = 445 nm, 88 mW/cm²) at 20 °C, with 5 μM catalyst, 0.2 mM $[Ru(bpy)_3](PF_6)_2$, 1M TEOA, 0.1 M HBF_4.
[b] $Mol_{H2}\, mol_{cat}^{-1}$.
[c] 7.2 μmol hydrogen detected in the blank experiment with no copper catalyst present. In contrast, no hydrogen was detected in the blank experiment done in the dark.

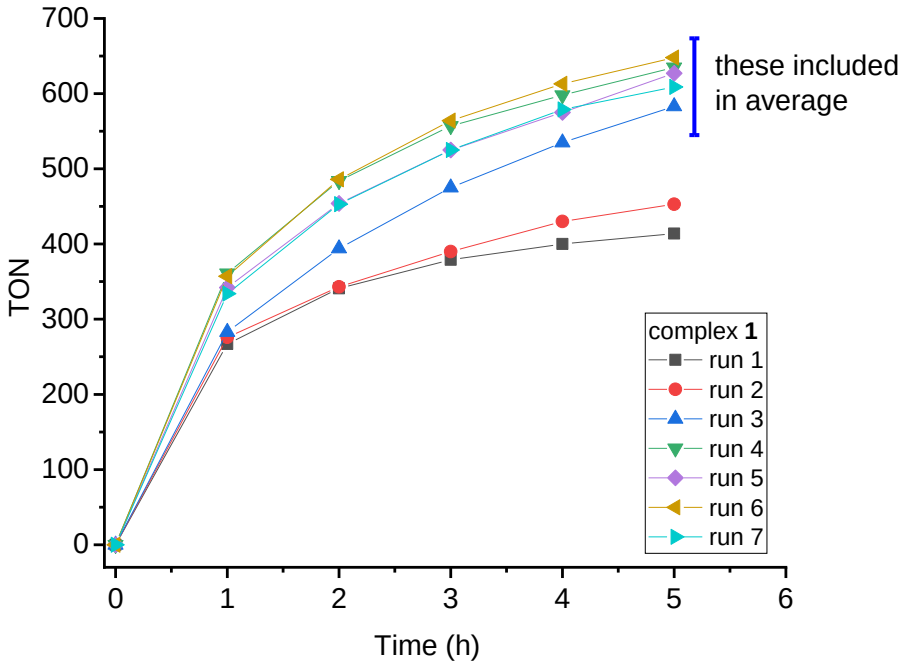

Figure S14. Reproducibility check of hydrogen TON vs time profile for copper complex **1** [Cu^{II} L^{Et}]BF_4 in DMF (C_{cat} = 5 μM) upon irradiation with a blue LED (λ = 445 nm, 88 mW/cm^2) at 20 °C, with 1.0 M TEOA, 0.2 mM [$Ru(bpy)_3$]$(PF_6)_2$ 0.1 M HBF_4 and 0.53 M of water. Runs 1 and 2 were carried out before the importance of using freshly prepared TEOA solution was realised (all subsequent runs used freshly prepared solutions) – as 3 day old solutions were used for runs 1 and 2, they have been excluded from the average (see Table S1).

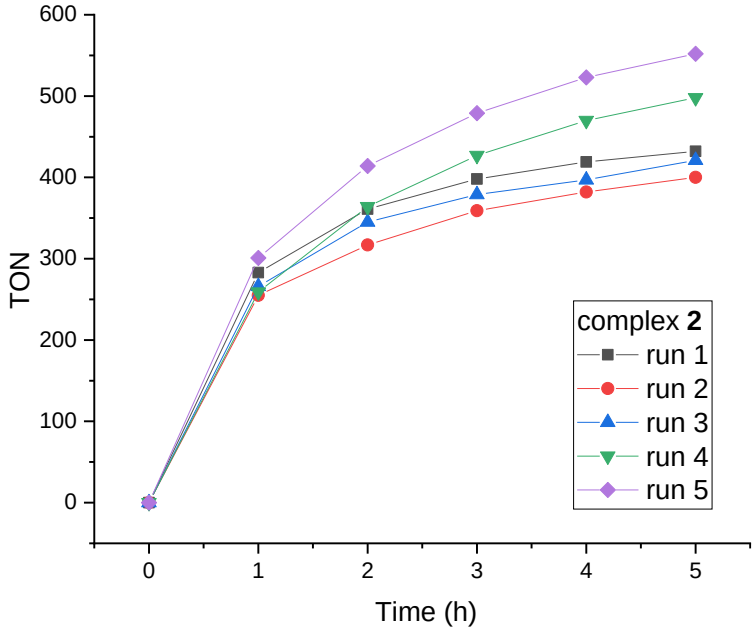

Figure S15. Reproducibility check of hydrogen TON vs time for copper complex **2** [Cu^{II} $L^{Et\text{-}MePy}$]BF_4 in DMF (C_{cat} = 5 μM) upon irradiation with a blue LED (λ = 445 nm, 88 mW/cm^2) at 20 °C, with 1.0 M TEOA, 0.2 mM [$Ru(bpy)_3$]$(PF_6)_2$ 0.1 M HBF_4 and 0.56 M of water. For completeness, please note that all five runs are included in the average (see Table S1).

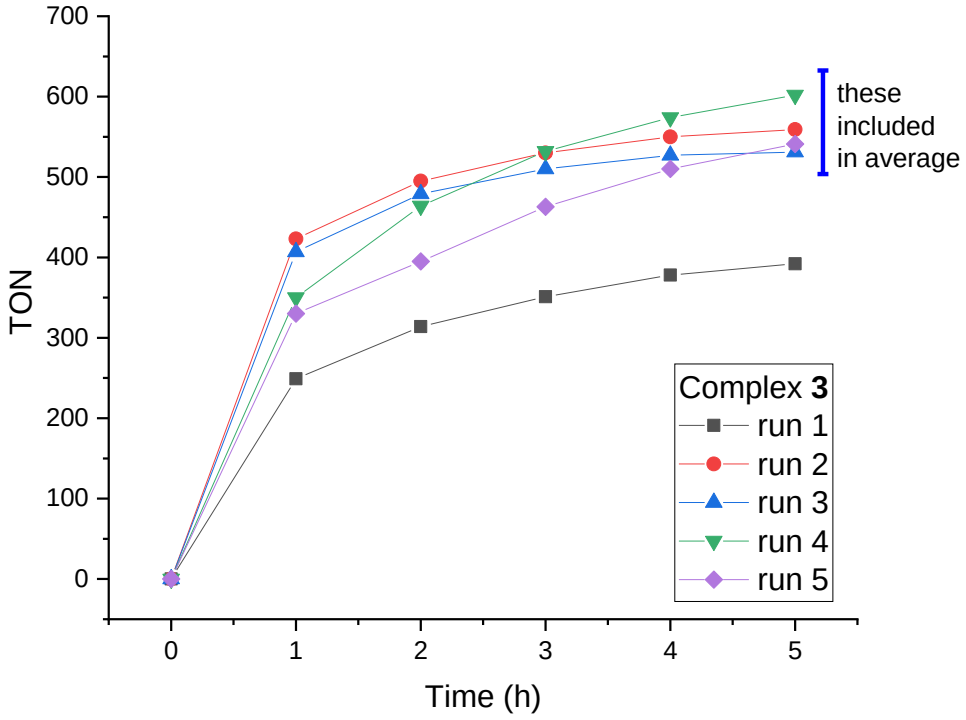

Figure S16. Reproducibility check of hydrogen TON vs time for copper complex **3** [Cu^{II} $\mathbf{L}^{EtPy2}$]BF_4 in DMF (C_{cat} = 5 μM) upon irradiation with a blue LED (λ = 445 nm, 88 mW/cm^2) at 20 °C, with 1.0 M TEOA, 0.2 mM $[Ru(bpy)_3](PF_6)_2$ and 0.1 M HBF_4 and 0.53 M of water. The intensity of the LED irradiation was observed to drop during run 1, so it was excluded from the average (see Table S1).

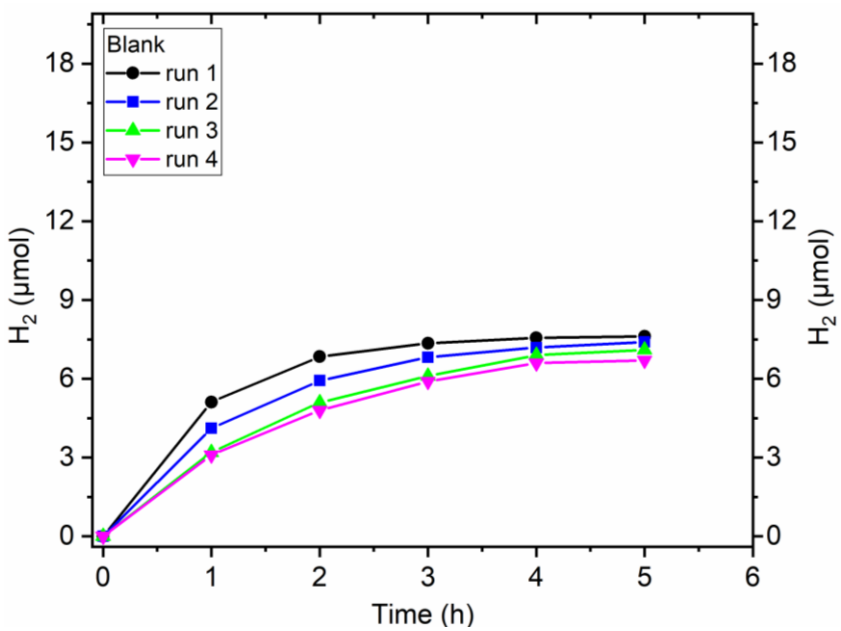

Figure S17. Reproducibility check of hydrogen TON vs time for blank experiments containing no copper catalyst, in DMF upon irradiation with a blue LED (λ = 445 nm, 88 mW/cm^2) at 20 °C, with 0.2 mM $[Ru(bpy)_3](PF_6)_2$, 1.0 M TEOA, 0.1 M HBF_4 and 0.53 M of water. TONs were calculated based on the moles of $[Ru(bpy)_3](PF_6)_2$ present in the experiment, but if calculated as if C_{cat} = 5 μM (note that is actually zero here) then TON_{Ru} = 7 gives a TON_{Cat} = 290.

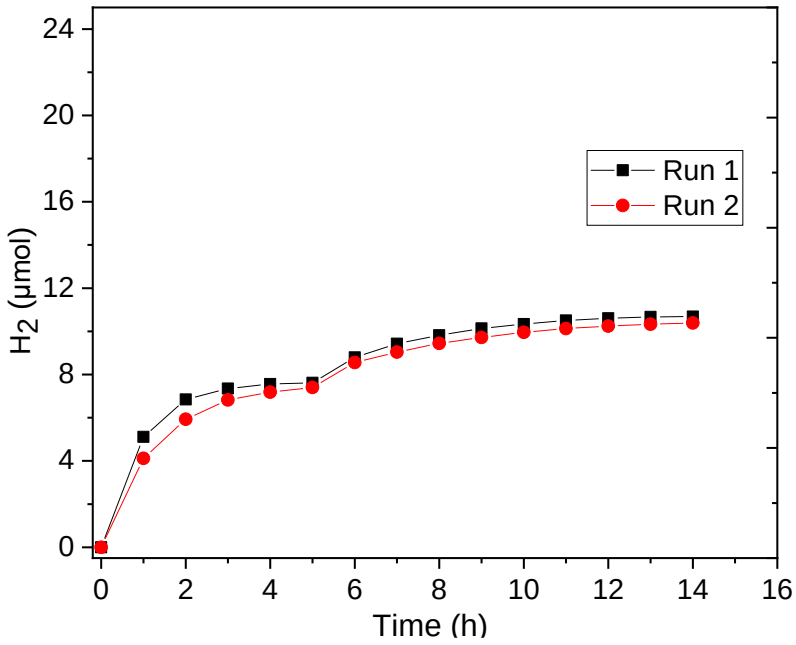

Figure S18. Hydrogen evolution (µmol) vs time profile for blank experiment containing no copper catalyst, in DMF, with duplicated runs, upon irradiation with a blue LED (λ = 445 nm, 88 mW/cm^2) at 20 °C, with 0.2 mM $[Ru(bpy)_3](PF_6)_2$, 1.0 M TEOA, 0.1 M HBF_4 and 0.53 M of water.

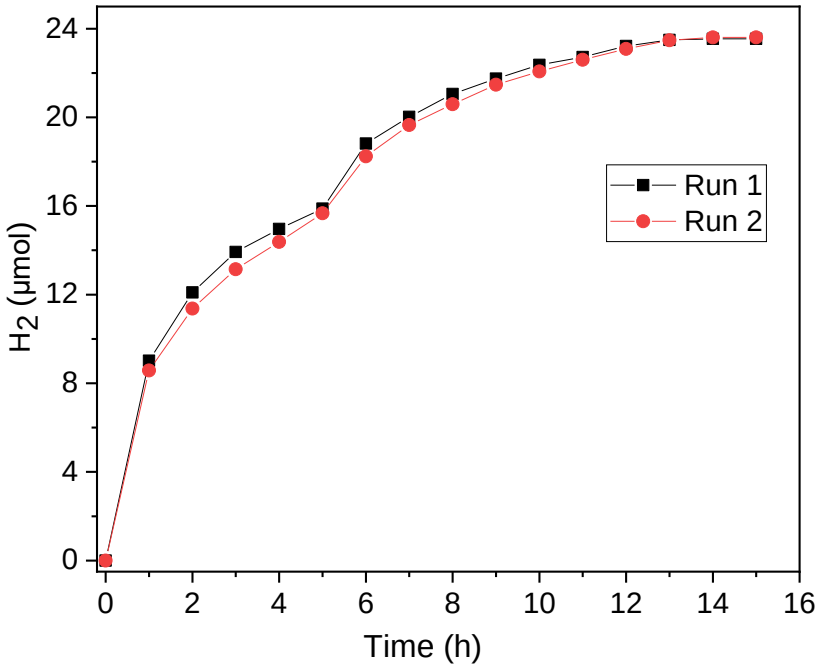

Figure S19. Hydrogen evolution (µmol) vs time profile for copper complex **1** $[Cu^{II}\mathbf{L}^{Et}]BF_4$ with duplicated runs, in DMF ($C_{cat.}$ = 5 µM) upon irradiation with a blue LED (λ = 445 nm, 88 mW/cm^2) at 20 °C, with 1.0 M TEOA, 0.2 mM $[Ru(bpy)_3](PF_6)_2$, 0.1 M HBF_4 and 0.53 M of water.

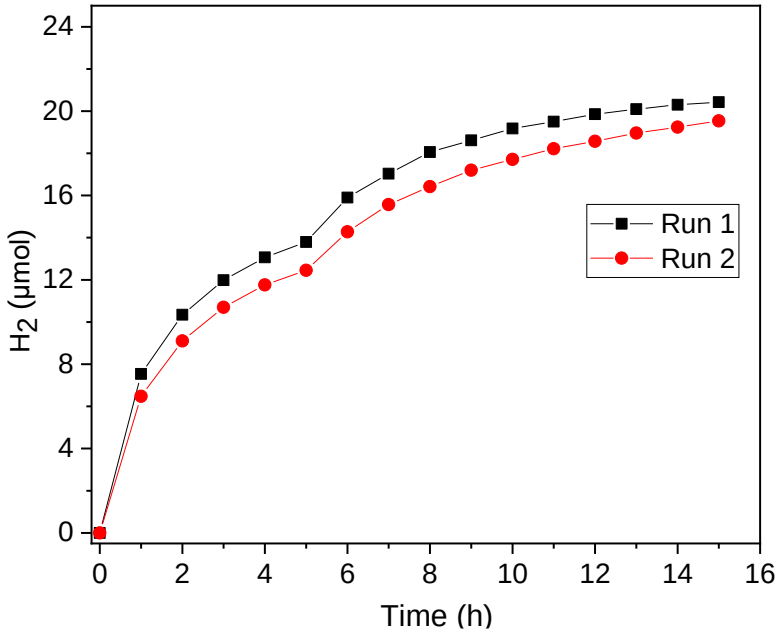

Figure S20. Hydrogen evolution (µmol) vs time profile for copper complex 2 [Cu^{II} **L**$^{Et\text{-}MePy}$]BF_4 with duplicated runs, in DMF ($C_{cat.}$ = 5 µM) upon irradiation with a blue LED (λ = 445 nm, 88 mW/cm^2) at 20 °C, with 1.0 M TEOA, 0.2 mM $[Ru(bpy)_3](PF_6)_2$, 0.1 M HBF_4 and 0.53 M of water.

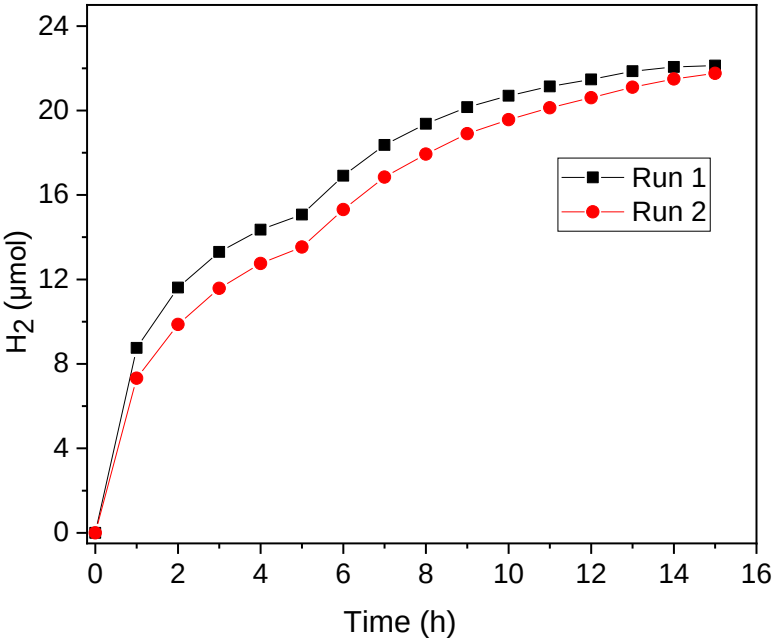

Figure S21. Hydrogen evolution (µmol) vs time profile for copper complex 3 [Cu^{II} **L**^{EtPy2}]BF_4, with duplicated runs, in DMF ($C_{cat.}$ = 5 µM) upon irradiation with a blue LED (λ = 445 nm, 88 mW/cm^2) at 20 °C, with 1.0 M TEOA, 0.2 mM $[Ru(bpy)_3](PF_6)_2$, 0.1 M HBF_4 and 0.53 M of water.

2. Electrochemistry and electrocatalytic HER

General method: All electrochemical measurements were carried out at the University of Otago by AA, in a three neck H-shaped electrochemical cell under an argon atmosphere (all solutions were purged with Ar for 20-30 min prior to study), using an IVIUMSATT.XRE potentiostat, a glassy carbon (3 mm diameter, surface area = 0.071 cm^2) as the working electrode, 0.01 M $AgNO_3$/Ag as the reference electrode, platinum sheet as the counter electrode. The working electrode compartment was filled with 8 mL of 0.1 M Bu_4NPF_6 acetonitrile solution, and the rest of the "H" was filled with ca. 10 mL of 0.1 M Bu_4NPF_6 acetonitrile solution.

Acetonitrile was freshly distilled over calcium hydride. Bu_4NPF_6 (99 %, for electrochemical analysis) was purchased from Sigma Aldrich and used without further purification.

The working electrode was cleaned before each measurement by: rinsing with water, ethanol and acetonitrile, then polishing with alumina slurry, and finally rinsing with acetonitrile and drying.

The three neck H-shaped electrochemical cell and Pt counter electrode were carefully cleaned and dried between studies as follows: filled and soaked in nitric acid (1 hour), rinsed thoroughly with copious water, filled and soaked in water (2 hours), rinsed with water, acetonitrile and acetone, soaked in dry MeCN for 24 hours, emptied and dried in an oven overnight before use.

Cyclic voltammetry (CV): CVs where carried out on 8 mL acetonitrile solutions that were 0.1 mM in **1**-**3** or the salt $Cu^{II}(BF_4)_2.xH_2O$, and 0.1 M in Bu_4NPF_6. Prior to each study, the purity of the electrolyte and solvent and the cleanliness of the cell setup was first checked by recording the CV from 0 to 2.0 to -2.0 to 0 V to confirm negligible background current was observed, before adding the respective copper complex and commencing the study. An internal reference check on the ferrocene/ferrocenium cation couple ($Fc^{+/0}$) was carried out at the conclusion of the CVs run on **1**-**3** in MeCN (no acid): it was consistently observed at $E_{1/2}(Fc^+/Fc)$ = 0.09 ± 0.01 V vs 0.01 M $AgNO_3$/Ag, with ΔE = 0.09 ± 0.01 V, vs 0.01 M $AgNO_3$/Ag.

Controlled potential electrolysis (CPE): CPE measurements were conducted using same cell described above, but in this case the working compartment was filled with 8 mL of 0.1 M Bu_4NPF_6 acetonitrile solution containing the specified amount of acid (0.08 M unless otherwise stated) and 1 mM in the copper complex, and the solution was efficiently stirred throughout CPE to ensure efficient mass transport (once we realised this was a problem in our first such experiments). The remainder of the 'H' was filled with ca. 10 mL of 0.1 M Bu_4NPF_6 acetonitrile solution. Our only available glassy carbon electrode (0.071 cm^2) and the 0.01 M $AgNO_3$/Ag reference electrode were placed into the working compartment, and the Pt sheet counter electrode was placed in the auxiliary compartment.

Additional reference electrode checks: Checks on the reference electrode before and after showed that no drift occurred during the experiments with acid present, including the 6 hour CPE experiments, as $E_{1/2}(Fc^+/Fc)$ = 0.09 ± 0.01 V vs 0.01 M $AgNO_3$/Ag, with ΔE = 0.09 ± 0.01 V, in all cases (see also Figure S25 right and Figure 32).

2.1 Cyclic voltammetry data (CVs)

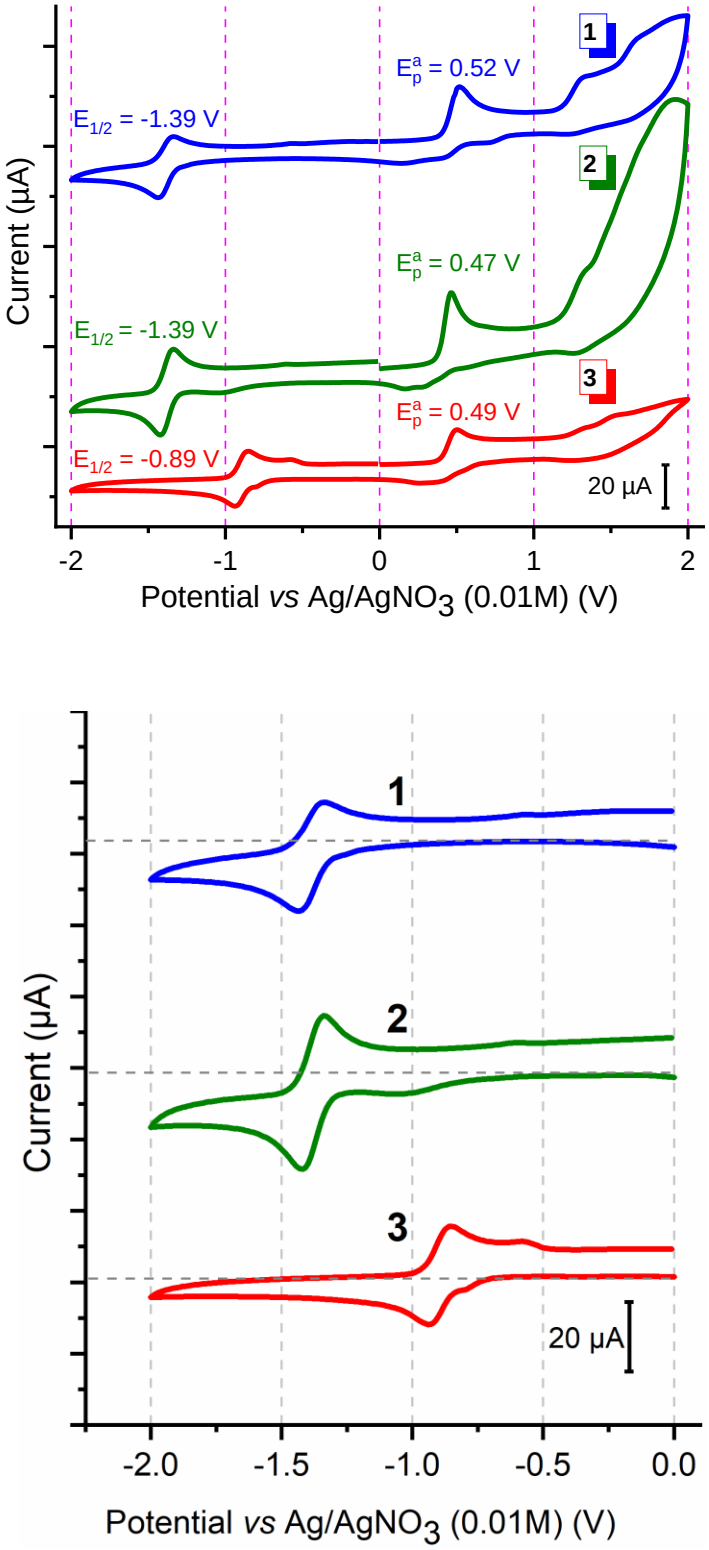

Figure S22. (Top) Full range CVs (E = 0→ +2→0→ -2→ 0 V) and (bottom) cathodic range CVs (E = 0→ -2→ 0 V) of an acetonitrile solution of (blue) 1 mM **1** $[Cu^{II}\,\mathbf{L}^{Et}]BF_4$ (green) 1.5 mM **2** $[Cu^{II}\,\mathbf{L}^{Et\text{-}MePy}]BF_4$ and (red) 1 mM **2** $[Cu^{II}\,\mathbf{L}^{EtPy2}]BF_4$. The CVs were collected vs 0.01 M $AgNO_3$/Ag, using 0.1 M $(Bu_4N)_4PF_6$ electrolyte, 3 mm glassy carbon (A = 0.071 cm^2 working electrode, scan rate of 100 mV/s and temperature of 20°C. Internal reference check $E_{1/2}(Fc^+/Fc)$ = 0.09 ± 0.01 V vs 0.01 M $AgNO_3$/Ag, with ΔE = 0.09 ± 0.01 V.

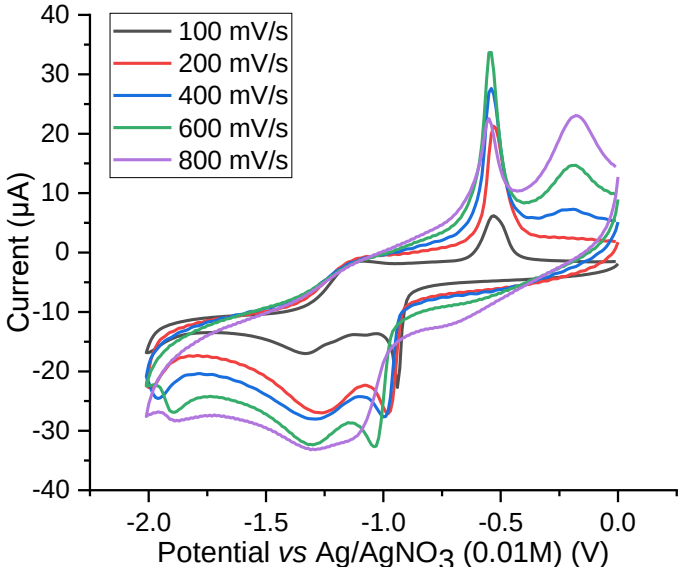

Figure S23. Cyclic voltammograms of 1 mM acetonitrile solution of $Cu(BF_4)_2.xH_2O$ at scan rate 100-800 mV/s, data was collected (E = 0→-2→0 V vs 0.01 M $AgNO_3$/Ag) using 0.1 M $(Bu_4N)_4PF_6$ as the electrolyte and 3 mm glassy carbon (A = 0.071 cm^2) as the working electrode at temperature 20° C. Internal reference check $E_{1/2}(Fc^+/Fc)$ = 0.09 ± 0.01 V vs 0.01 M $AgNO_3$/Ag, with ΔE = 0.09 ± 0.01 V.

Table S2. Electrochemical parameters extracted form cyclic voltammetry data of complexes **1**-**3** at different scan rates (Figure 7). Conditions: 0.1 M $(Bu_4N)PF_6$, glassy carbon working electrode (*d* = 3 mm, *A* = 0.071 cm^2), 293 K, vs 0.01 M $AgNO_3$/Ag.

complex	Scan rate (mV/s)	E_c (V)	E_a (V)	$E_{1/2}$ (V)	ΔE (V)	i_c (μA)	i_a (μA)	I_a/i_c
1	50	-1.43	-1.34	-1.39	0.09	-14.7	14.1	0.96
	100	-1.43	-1.34	-1.39	0.09	-18.9	18.5	0.98
	200	-1.43	-1.34	-1.39	0.09	-27.6	27.8	1.01
	400	-1.43	-1.34	-1.39	0.09	-41.4	39.7	0.96
2	50	-1.43	-1.34	-1.39	0.09	-7.6	8.2	1.08
	100	-1.43	-1.34	-1.39	0.09	-11.4	11.5	1.01
	200	-1.42	-1.34	-1.38	0.08	-16.1	16.5	1.02
	400	-1.43	-1.34	-1.39	0.09	-21.0	21.5	1.02
3	50	-0.94	-0.85	-0.89	0.09	-17.1	16.3	0.95
	100	-0.94	-0.85	-0.89	0.09	-25.2	24.5	0.97
	200	-0.94	-0.85	-0.89	0.08	-32.9	34.5	1.05
	400	-0.94	-0.85	-0.89	0.09	-45.8	43.7	0.95

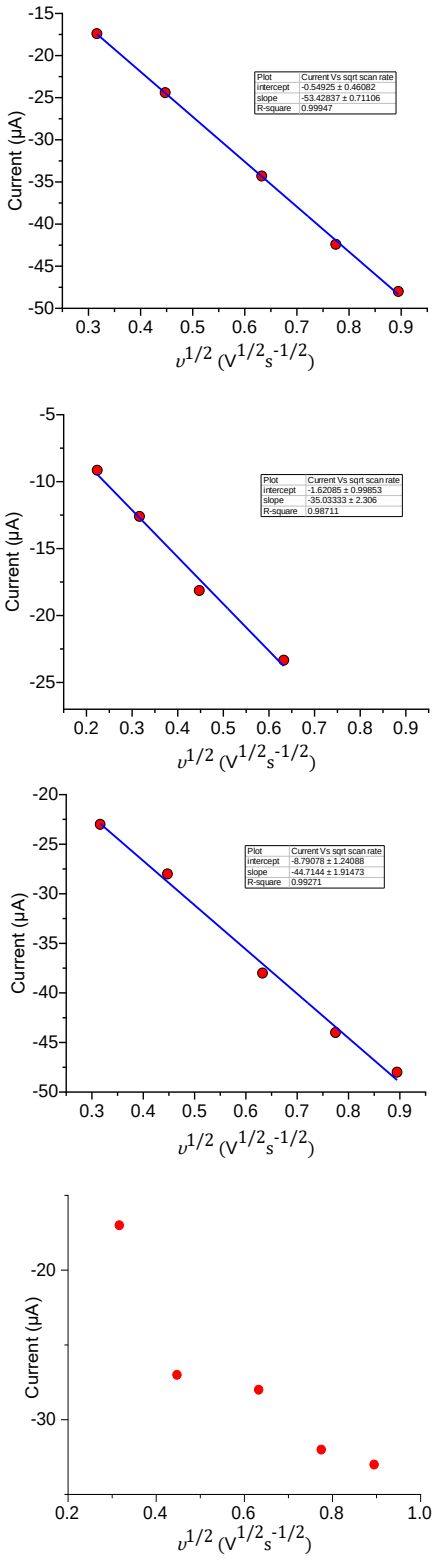

Figure S24. Plot of catholic peak current versus the square root of the scan rate ($\upsilon^{1/2}$) of the reversible redox event for 1 mM acetonitrile solution of (from up to bottom) (up) compound **1** $[Cu^{II}\,\mathbf{L}^{Et}]BF_4$ ($E_{1/2}$ = -1.38 V, ΔE = 0.09 ± 0.01) Diffusion coefficient (*D*) = 7.7 x 10^{-6} cm^2s^{-1}, **2** $[Cu^{II}\,\mathbf{L}^{Et\text{-}MePy}]BF_4$ ($E_{1/2}$ = -1.39 V, ΔE = 0.09 ± 0.01) *D* = 3.3 x 10^{-6} cm^2s^{-1}, **3** $[Cu^{II}\,\mathbf{L}^{EtPy2}]BF_4$ ($E_{1/2}$ = -0.85 V, ΔE = 0.09 ± 0.01) *D* = 5.4 x 10^{-6} cm^2s^{-1} and (bottom) the $Cu(BF_4)_2.xH_2O$. Conditions: Electrolyte; 0.1 M $(Bu_4N)PF_6$, working electrode; 3 mm glassy carbon (A = 0.071 cm^2), 20° C. All three of the 'best fit' lines (blue) have R^2 of 0.99-1.00.

To calculate the diffusion coefficient, *D*, the Randles–Sevcik equation[6] is:

$$i_p = 0.4463nFAC^0\left(\frac{nF\upsilon D}{RT}\right)^{\frac{1}{2}} \quad (1)$$

Where
i_p is the peak current (A),
n is number of electrons transferred,
A is electrode surface area (cm^2),
C^0 is analyte concentration (mol cm^{-3}),
υ is scan rate (V/s),
D is diffusion coefficient ($cm^2\ s^{-1}$),
F is Faraday's constant (C mol^{-1}),
R is gas constant (J K^{-1} mol^{-1}) and
T is temperature (K).

Rearranging eqn 1 slightly gives:

$$i_p = \left[0.4463nFAC^0\left(\frac{nFD}{RT}\right)^{1/2}\right]\upsilon^{\frac{1}{2}}$$

So the slope of a plot of i_p versus $\upsilon^{\frac{1}{2}}$ is given by:

$$slope = 0.4463nFAC^0\left(\frac{nFD}{RT}\right)^{\frac{1}{2}} \quad (2)$$

Enabling easy calculation of *D* the diffusion coefficient from the slope by rearranging eqn 2:

$$D = \left(\frac{slope}{0.4463nFAC^0}\right)^2\frac{RT}{nF}$$

Then substituting n = 1, A = 0.071 cm^2, C^0 = 1x10^{-6} (mol cm^{-3}), F = 96,485 (C mol^{-1}), R = 8.314(J K^{-1} mol^{-1} and T = 293 K:

$$\underline{D = 2700\ (slope)^2\ \text{cm}^2\text{s}^{-1}}$$

For **1** $[Cu^{II}\mathbf{L}^{Et}]BF_4$

Equation of best fit line in plot of i_p versus $\upsilon^{\frac{1}{2}}$ (Figure S24) is: $y = -0.55 - 53x$
So slope = -53 giving D = 7.7 x 10^{-6} cm^2s^{-1}

For **2** $[Cu^{II}\mathbf{L}^{Et\text{-}MePy}]BF_4$

Equation of best fit line in plot of i_p versus $\upsilon^{\frac{1}{2}}$ (Figure S24) is: $y = -1.6 - 35x$
So slope = -35, giving D = 3.3 x 10^{-6} cm^2s^{-1}

For **3** $[Cu^{II}\mathbf{L}^{EtPy2}]BF_4$

Equation of best fit line in plot of i_p versus $\upsilon^{\frac{1}{2}}$ (Figure S24) is: $y = -8.8 - 45x$
So slope = -45, giving D = 5.4 x 10^{-6} cm^2s^{-1}

2.2 CVs with successive acetic acid addition

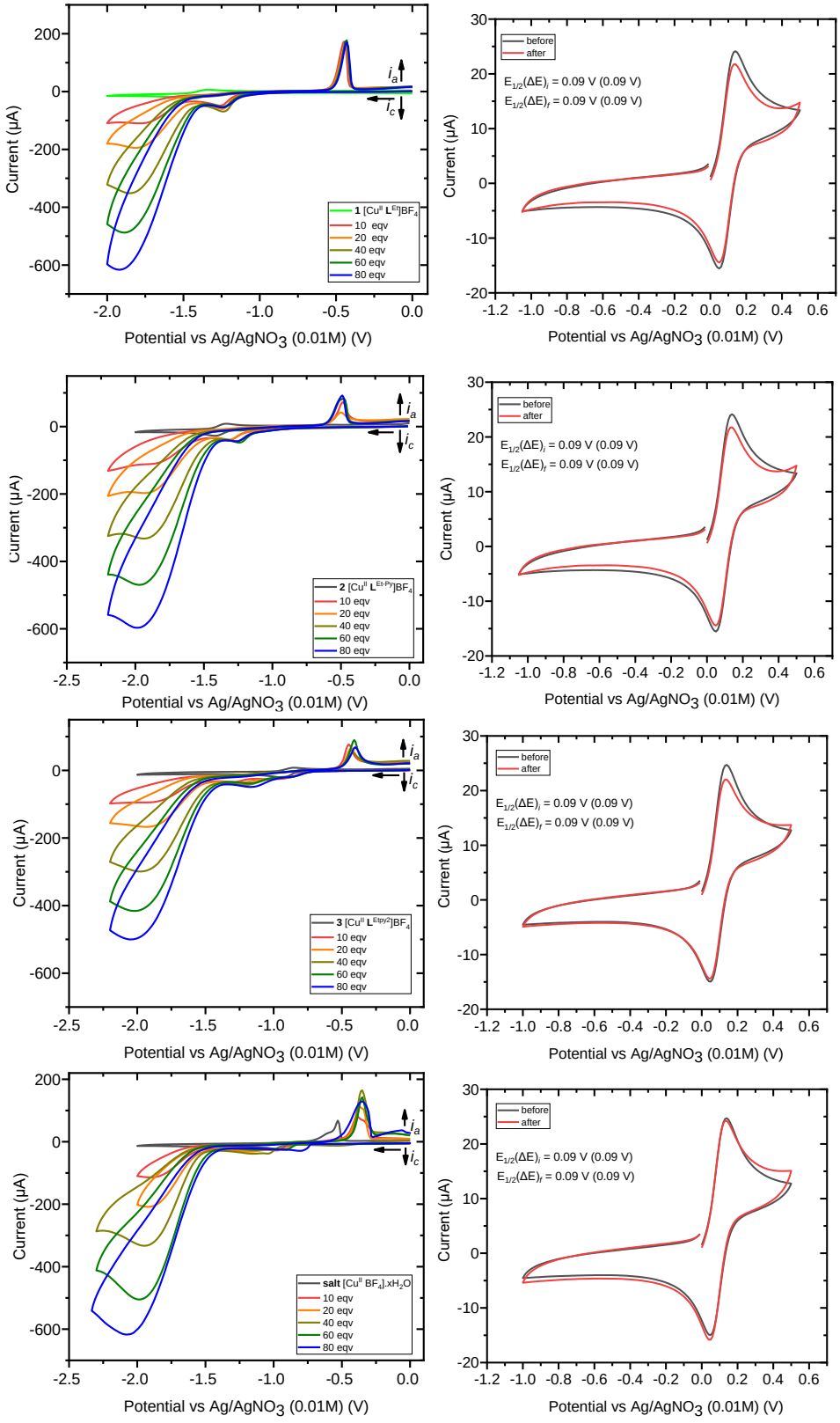

Figure S25. (Left) Cyclic voltammograms of 1 mM of (from top to bottom) **1** $[Cu^{II}L^{Et}]BF_4$, **2** $[Cu^{II}L^{Et\text{-}Mepy}]BF_4$, **3** $[Cu^{II}L^{Etpy2}]BF_4$ and $Cu(BF_4)_2.xH_2O$ salt in acetonitrile with successive additions of acetic acid, vs 0.01 M $AgNO_3$/Ag. (Right) In all cases, the before and after reference checks prove there is no drift: $E_{1/2}(Fc^+/Fc)$ = 0.09 ± 0.01 V vs 0.01 M $AgNO_3$/Ag, with ΔE = 0.09 ± 0.01 V. Conditions: 0.1 M $(Bu_4N)PF_6$, 3 mm glassy carbon working (A = 0.071 cm^2) and Pt counter electrode, 100 mV/s, 20°C.

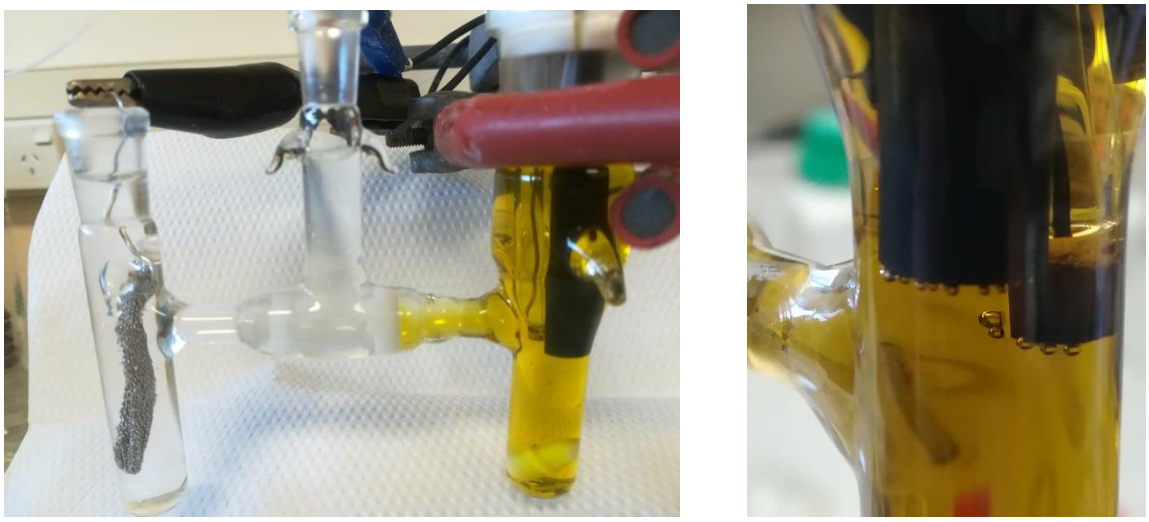

Figure S26. (Left) Electrochemical "H" cell (design details and training kindly provided in 1996 by Dr E. Bothe, MPI für Strahlenchemie, Mulheim an der Ruhr, Germany, to SB when she was there on sabbatical leave as a Humboldt Fellow) used for bulk electrolysis experiments. (Right) Evolution of bubbles already visible on the 3 mm glassy carbon working electrode (A =0.071 cm^2) within the first 2 minutes of controlled potential electrolysis at E = -1.6 V vs 0.01 M $AgNO_3$/Ag, of 1 mM of complex $[Cu^{II}\,\mathbf{L}^{Et}]BF_4$ **1** in presence of 80 mM acetic acid. Conditions: 20° C, Pt sheet counter electrode. Checks on the reference electrode before and after showed that no drift occurred in the reference electrode during these experiments, as $E_{1/2}(Fc^+/Fc)$ = 0.09 ± 0.01 V vs 0.01 M $AgNO_3$/Ag, with ΔE = 0.09 ± 0.01 V, in all cases (see also Figure S25, right).

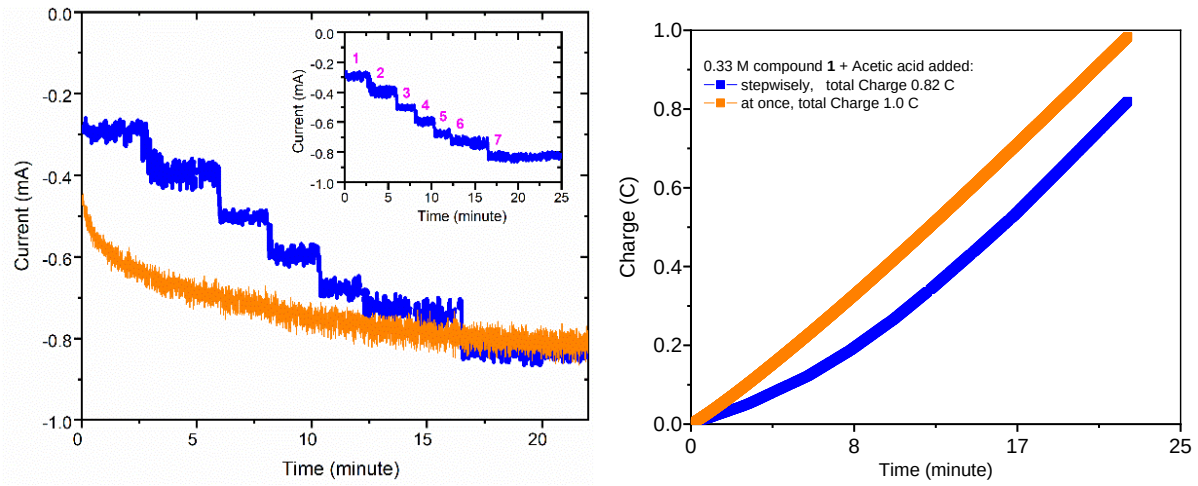

Figure S27. (Left) Plot of current response versus time during electrolysis at $E_{applied}$ = -1.6 V vs 0.01 M $AgNO_3$/Ag for a 0.33 M acetonitrile solution of **1** when the acetic acid is either (blue) added in 7 portions reaching 80 mM in H^+ after the 7th addition or (orange) it is 80 mM from the start; the inset displays the stepwise acid addition experiment more clearly than in the main plot. (Right) The corresponding charge building up during the two electrolysis processes shown on the left. Conditions: glassy carbon working electrode (*d* = 3 mm, *A* = 0.071 cm^2), 20° C, and Pt counter electrode.

Table S3. Summary of key data, including charge and e-equivalents transferred plus TON(H_2), obtained during controlled potential electrolysis at -1.60 V of an 8 mL solution of 80 mM acetic acid in the presence of **1**, for the runs detailed and plotted in Figure 10 (runs 1-3 in this table) and Figure 11 (runs 4 and 5 in this table).

Description		Charge (C)	# of e's per **1**	TON(H_2)
Run 1 (blue line, Figure 10)	2 hour	7.2	9.3	4.7
	6 hour	18.7	24.2	12.1
Run 2 (violet line, Figure 10)	2 hour	7.4	9.6	4.8
	6 hour	19.9	25.8	12.9
Run 3 - + mercury drop (sky blue line, Figure 10)	2 hour	7.2	9.3	4.7
	6 hour	17.0	22.0	11.0
Run 4 - stepwise acid addition (blue line, Figure 11)	25 min	0.82	3.2	1.6
Run 5 - 80 mM acid from start (orange line, Figure 11 and S27)	25 min	1.0	3.9	1.9

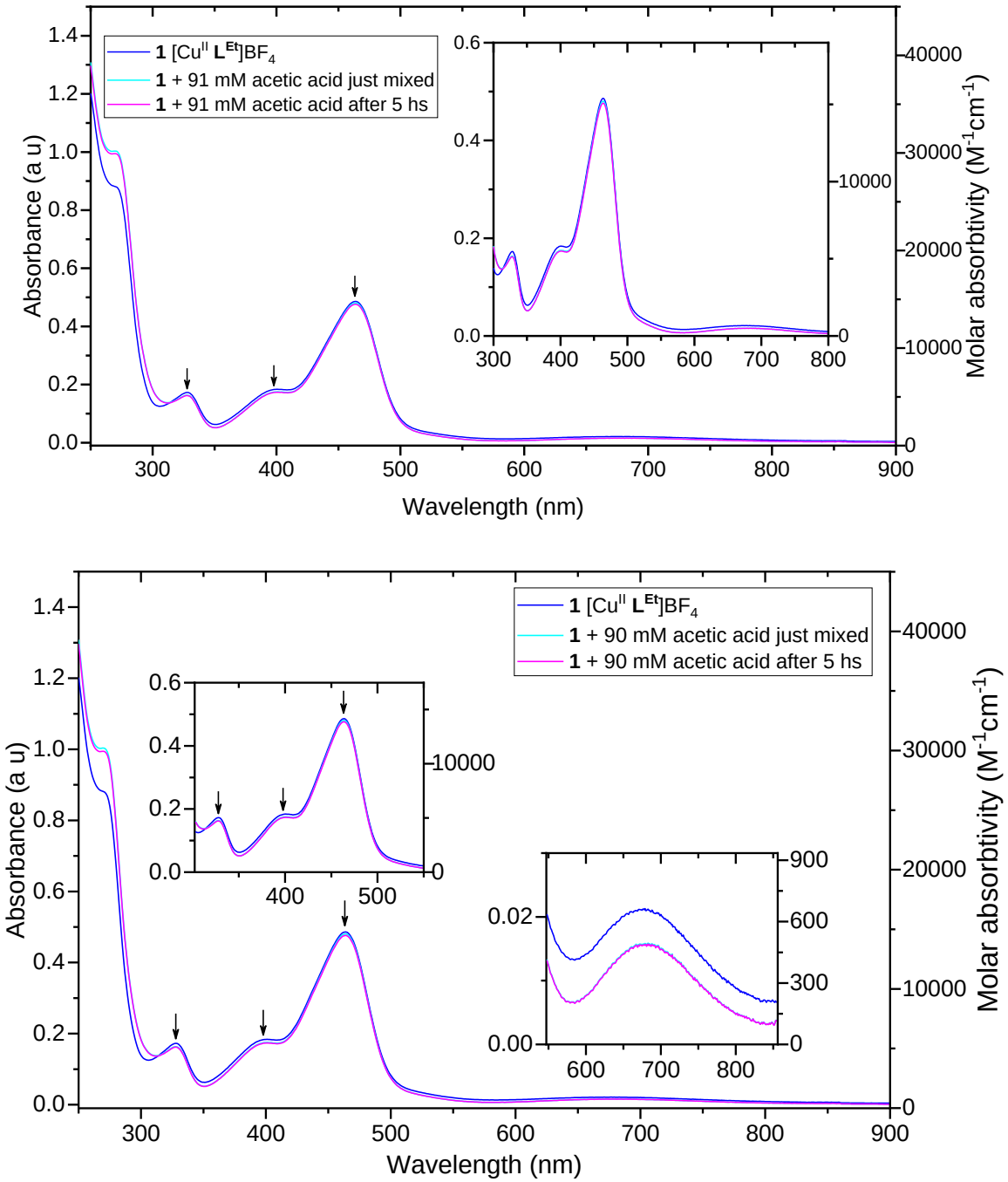

Figure S28. Two plots, showing expansions of different regions, of the same UV-vis absorption spectra of a 0.032 mM solution of [Cu^{II} **L**^{Et}]BF$_4$ **1**, prepared in 0.1 M of Bu$_4$NPF$_6$ acetonitrile solution in the presence of 90 mM acetic acid (aqua) at the moment of mixing and (magenta) at 5 hours in air after mixing, and of (blue line) an identical solution in the absence of acid. Inset; expansion of the 300-800 cm^{-1} region.

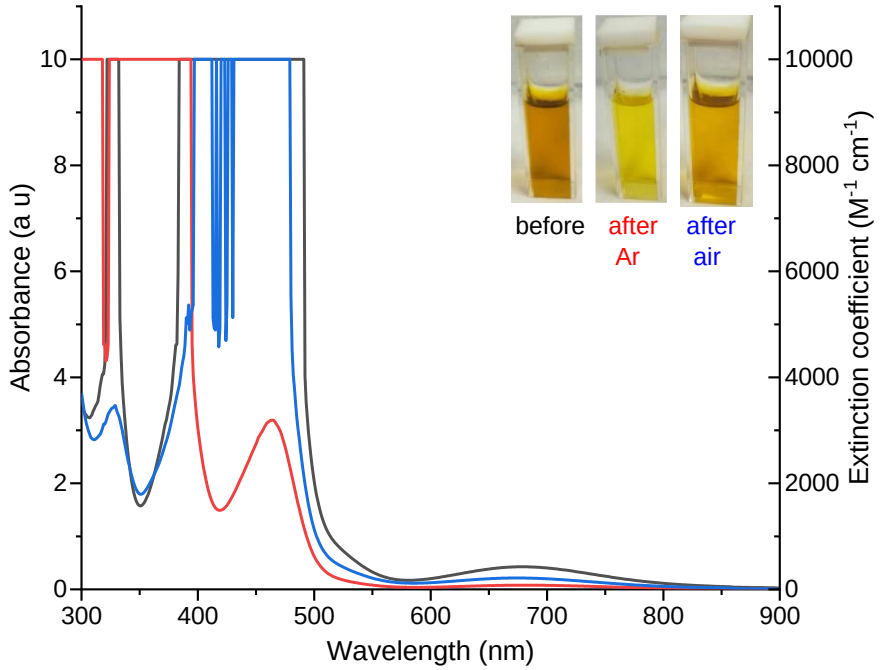

Figure S29. UV-vis spectra, of 1 mM $[Cu^{II}L^{Et}]BF_4$ (**1**) in the presence of 80 mM acetic acid in 0.1 M Bu_4NPF_6/MeCN (black) before electrolysis commenced, (red) immediately after 6 hours electrolysis, and then (blue) after the post-electrolysis solution was exposed to air for 30 minutes. Electrolysis conditions: glassy carbon working electrode (d = 3 mm, A =0.071 cm^2), 20° C, and Pt counter electrode.

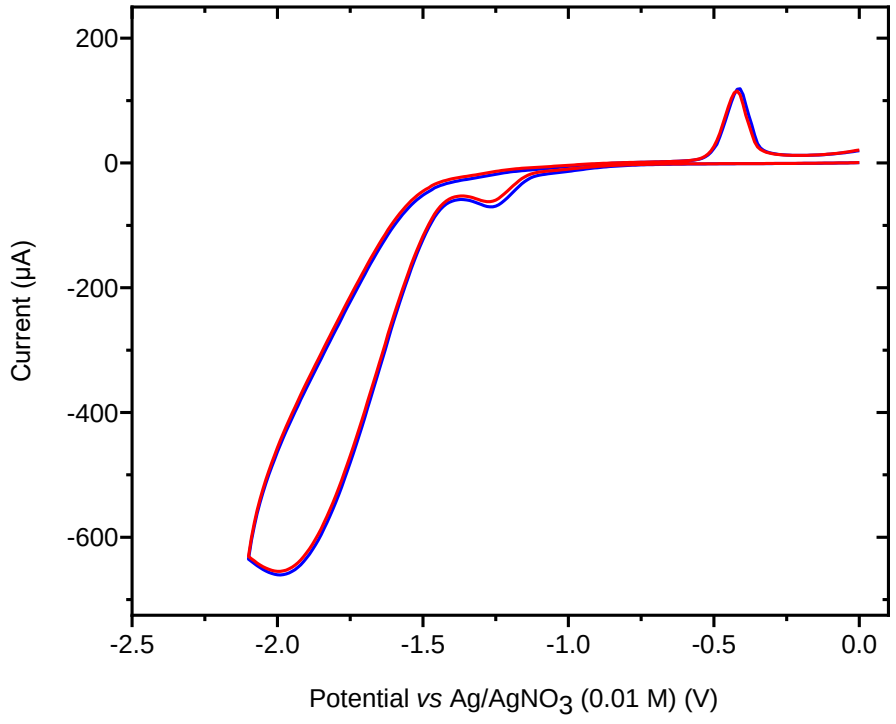

Figure S30. Cyclic voltammetry, 0→ -2.0→ 0 V vs 0.01 M $AgNO_3$/Ag, for a 1 mM MeCN solution of **1**, in presence of 80 mM of acetic acid, in (blue) the absence of mercury and (red) the presence of 1 mL of mercury. Conditions: 0.1 M $(NBu_4)PF_6$, glassy carbon working electrode (d = 3 mm, A = 0.071 cm^2), 293 K, scan rate 100 mVs^{-1}.

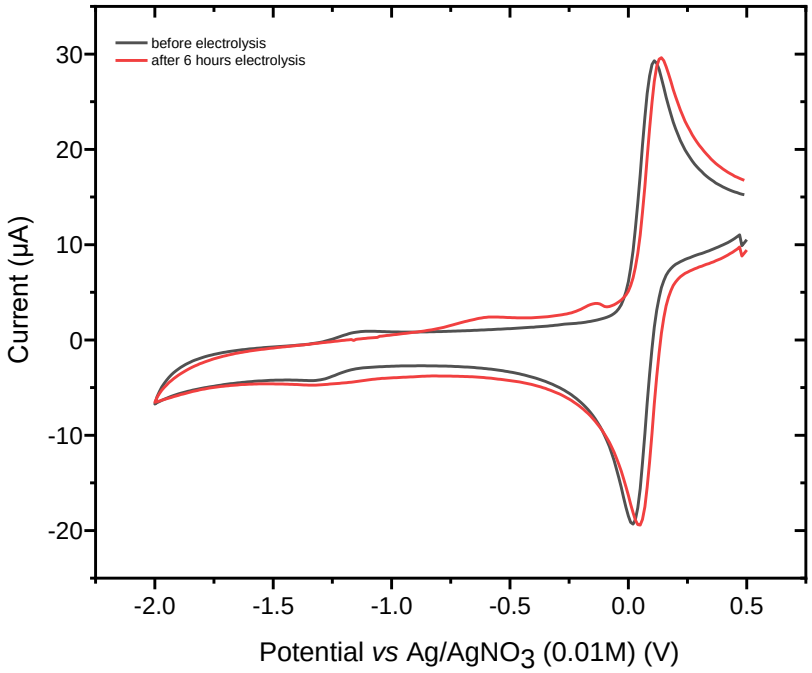

Figure S31. CV of the reference electrode (0.01 M $Ag/AgNO_3$) versus 1 mM Fc^+/Fc measured in 0.1 M Bu_4NPF_6 acetonitrile: (black) before, (red) after 6 hours controlled potential electrolysis of 80 mM acetic acid in the presence of **1**. Conditions: 0.1 M $(NBu_4)PF_6$, glassy carbon working electrode (d = 3 mm, A = 0.071 cm^2), 293 K, scan rate 100 mVs^{-1}. $E_{1/2}(Fc^+/Fc)$ = 0.09 ± 0.01 V vs 0.01 M $AgNO_3/Ag$, with ΔE = 0.09 ± 0.01 V, both before and after.

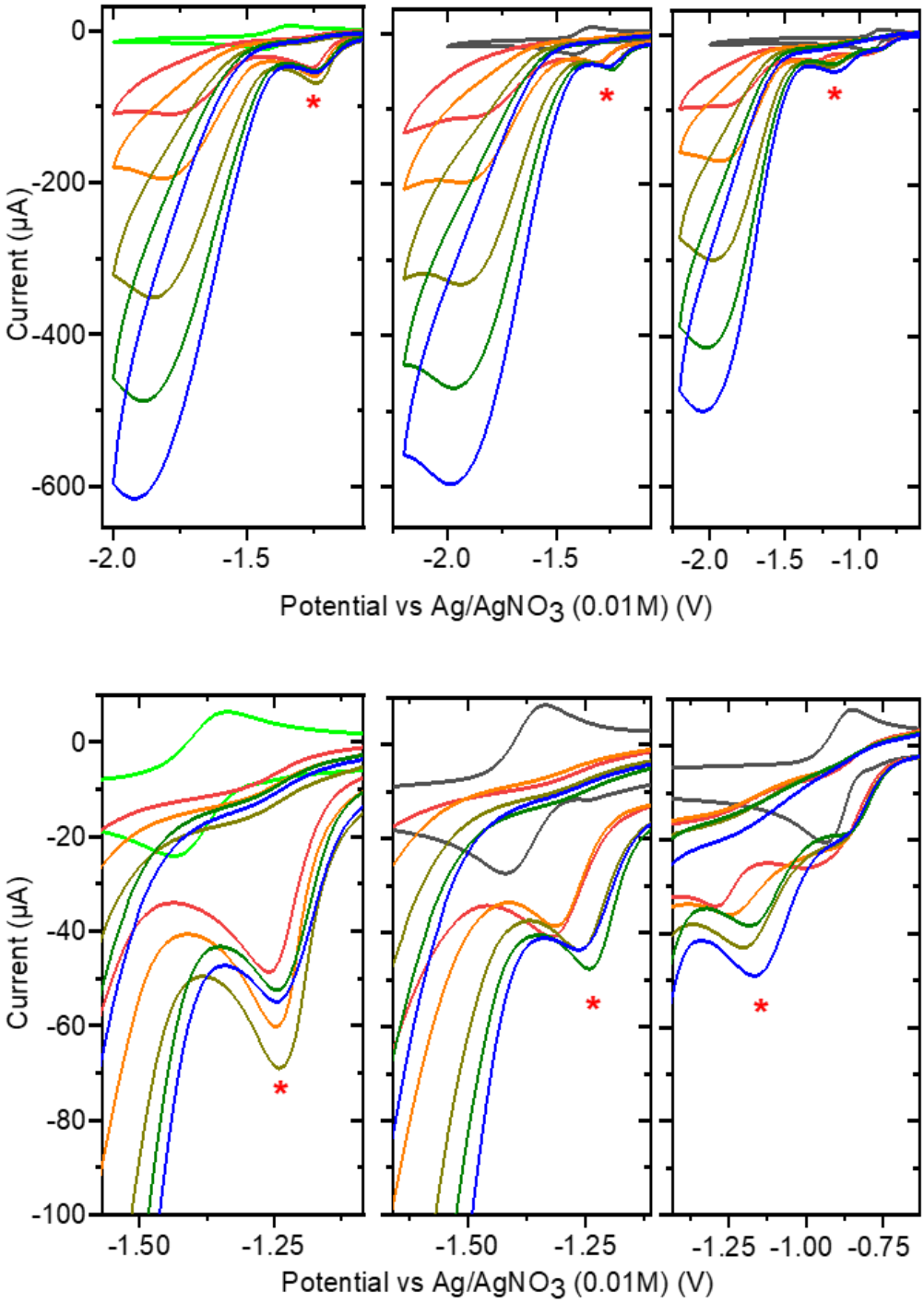

Figure S32. Cyclic voltammetry, 0→ -2.0 → 0 V vs 0.01 M $AgNO_3$/Ag showing (top) both catalytic and precatalytic wave (red star, occurs at -1.24→ -1.26 V for **1**, -1.33 V → -1.24 V for **2** and -1.25 V→ -1.17 V for **3**) and (bottom) enlarge region of the precatalytic wave, for a 1 mM MeCN solution of, from left to right: **1** (light green, no acid), **2** (gray, no acid) and **3** (gray, no acid), with successive additions of acetic acid (10 mM red, 20 mM orange, 40 mM dark yellow, 60 mM olive and 80 mM blue). Conditions: 0.1 M $(NBu_4)PF_6$, glassy carbon working electrode (d = 3 mm, A = 0.071 cm^2), 293 K, scan rate 100 mVs^{-1}. Before and after this study, $E_{1/2}(Fc^+/Fc)$ = 0.09 ± 0.01 V, with ΔE = 0.09± 0.01 V (Figure S25).

Table S4. Analysis of the catalytic, precatalytic and stripping wave, as a function of acetic acid concentration, observed in the CVs at 100 mV/s of a dry MeCN solution containing 1 mM of the chosen copper catalyst (Figure S32; details as per that caption). i_p^0 is the peak current of the Cu(II)/Cu(I) wave (marked with a *) in the absence of acetic acid; i_p is the peak current, and E_p is the corresponding voltage (vs 0.01 M $AgNO_3$/Ag) of the wave in the presence of acetic acid at the concentrations noted in the table.

Compound 1	Catalytic wave (Figure S25)	Precatalytic wave (Figure S32); * indicates Cu(II)/Cu(I) – no acid			Stripping peak (Figure S33)
[acetic acid] /mM	i_p/ µA (E_p / V)	i_p/ µA (E_p / V)	i_p/i_p^0	$(\frac{i_p}{i_p^0}-1)$	i_a/ µA (E_a / V)
0		-24 (-1.43)*	1.0	0.0	-
10	-109 (-1.78)	-49 (-1.26)	2.0	1.0	172 (-0.45)
20	-196 (-1.80)	-60 (-1.25)	2.5	1.5	160 (-0.44)
40	-353 (-1.85)	-69 (-1.25)	2.9	1.9	172 (-0.43)
60	-488 (-1.88)	-52 (-1.25)	2.2	1.2	176 (-0.43)
80	-618 (-1.92)	-55 (-1.24)	2.3	1.3	171 (-0.43)
Compound 2					
[acetic acid] /mM					
0		-27 (-1.42)*	1.0	0.0	-
10	-110 (-1.91)	-41 (-1.33)	1.5	0.5	41 (-0.50)
20	-196 (-1.93)	-38 (-1.31)	1.4	0.4	73 (-0.48)
40	-343 (-1.95)	-44 (-1.26)	1.6	0.6	82 (-0.49)
60	-470 (-1.96)	-48 (-1.24)	1.8	0.8	73 (-0.48)
80	-599 (-2.00)	-44 (-1.26)	1.6	0.6	92 (-0.50)
Compound 3					
[acetic acid] /mM					
0		-20 (-0.93)*	1.0	0.0	-
10	-94 (-1.92)	-36 (-1.25)	1.7	0.7	77 (-0.45)
20	-167 (-1.93)	-34 (-1.29)	1.8	0.8	65 (-0.43)
40	-296 (-1.97)	-43 (-1.21)	2.2	1.2	51 (-0.42)
60	-415 (-2.00)	38 (-1.18)	1.9	0.9	89 (-0.41)
80	-500 (-2.04)	49 (-1.17)	2.5	1.5	69 (-0.40)

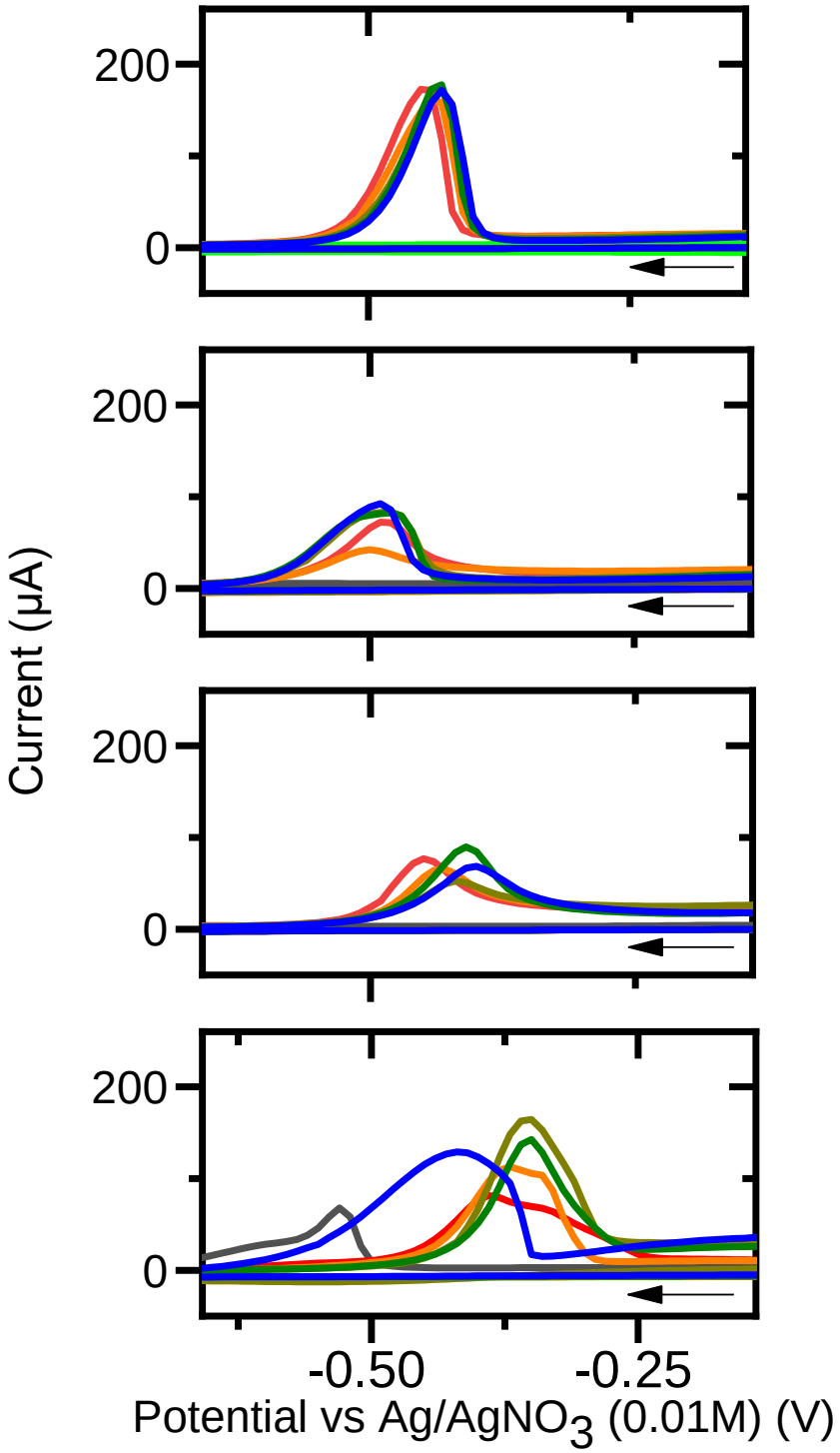

Figure S33. Enlargement of the stripping peak region, observed on the reverse scan (black arrow shows the forward scan), in the CVs shown in Figure S25, at 100 mV/s of a dry MeCN solution containing 1 mM of, 0→ -2.0 → 0 V vs 0.01 M $AgNO_3$/Ag), for a 1 mM MeCN solution of, from top to bottom: **1**, **2**, **3** and free copper(II) salt, with successive additions of acetic acid (10 mM red, 20 mM orange, 40 mM dark yellow, 60 mM olive and 80 mM blue). Conditions: 0.1 M $(NBu_4)PF_6$, glassy carbon working electrode (d = 3 mm, A = 0.071 cm^2), 293 K, scan rate 100 mVs^{-1}. Before and after this study, $E_{1/2}(Fc^+/Fc)$ = 0.09 ± 0.01 V, with ΔE = 0.09 ± 0.01 V.

Preparation of HL^{Et} macrocycle HL^{Et}

The Schiff base macrocycle H**L**^{Et} was prepared in same manner as our previously reported synthesis.[7, 8] The typical procedure is as follows.

Dpa (0.207 g, 0.92 mmol)[7, 9] was dissolved in a boiling MeCN (40 mL) producing a bright yellow solution. Diethylenediamine (0.095 g, 0.92 mmol, 1 equivalent) was then added and the resulting solution was refluxed for 3 hours. The reaction mixture was taken to dryness, resulting in a yellow oily product in a quantitative yield. Drying under high vacuum for 5 h produced H**L**^{Et} as a shiny yellow crystalline solid (0.28 mg, 95%).

Microanalysis calcd for $C_{18}H_{20}N_4.0.5H_2O$ (%): C, 71.73; H, 7.02; N, 18.59.
Found: C, 72.13; H, 6.96; N, 18.26.

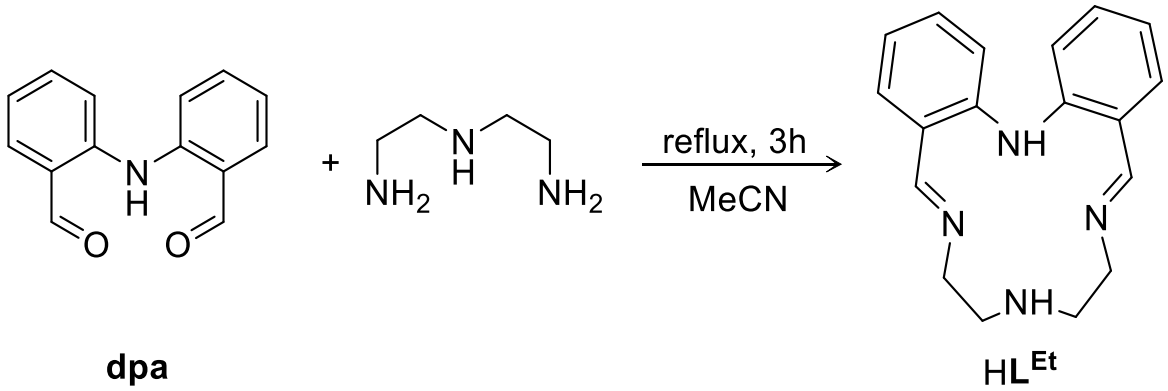

dpa HL^{Et}

Figure S34. Preparation of the N4-donor [1+1] Schiff base macrocycle, as reported previously.[7, 8] Note that **dpa** was also prepared as reported in the literature.[7, 9]

3. X-ray crystal structures

X-ray crystallographic data was collected on an Oxford Diffraction SuperNova diffractometer with Atlas CCD, equipped with a Cryostream N_2 open-flow cooling device, using mirror monochromated micro-focus Cu-*Kα* radiation at 100 K. A complete set of unique reflections to a maximum resolution of 0.82 Å was collected. Raw frame data (including data reduction, inter-frame scaling, unit cell refinement and absorption corrections) for all structures were processed using *CrysAlis Pro.*[10] Structures were solved and refined against all F^2 data using *SHELXL-2014*:[11] *OLEX2*[12] was used as the interface to visualise the structure during the refinement process. All non-H atoms were refined anisotropically. Hydrogen atoms were inserted at calculated positions with U(H) = 1.2 U(attached atom). High resolution pictures were prepared using Mercury[13] and POVray[14] software.

$[Cu^{II}\,L^{Et\text{-}Py}]BF_4$ (2). Dark red needle shaped crystal. Two fluorines (F12 and F13) of BF_4 showed signs of disorder (large ellipsoids) but as this involved only two atoms this could not modelled satisfactorily and instead it was left with higher thermal ellipsoids for those atoms.

$[Cu^{II}\,L^{EtPy2}](BF_4)$ (3). Dark red needle shaped crystal.

Table S5. Crystal data and structure refinement details for the complexes $[Cu^{II}\mathbf{L}^{Et\text{-}Py}]BF_4 \cdot H_2O$ (**2**) and $[Cu^{II}L^{EtPy2}](BF_4)$ (**3**).

	$[Cu^{II}\,\mathbf{L}^{Et\text{-}Py}]BF_4$, **2**	*$[Cu^{II}\,\mathbf{L}^{EtPy2}](BF_4)$*, **3**
Empirical formula	$C_{24}H_{24}BCuF_4N_5$	$C_{28}H_{26}BCuF_4N_5$
M_r	532.83	582.89
Crystal system	monoclinic	monoclinic
Space group	*$P2_1/n$*	*$P2_1/n$*
a [Å]	10.1780(7)	15.2239(6)
b [Å]	18.9792(9)	8.5237(4)
c [Å]	11.7456(0)	20.9758(11)
α [°]	90	90
β [°]	91.602(8)	110.841(6)
γ [°]	90	90
V [Å^3]	2268.0(3)	2543.8(2)
Z	4	4
T [K]	100(2)	100(2)
$\rho_{calcd.}$ [g/cm^3]	1.560	1.540
μ [mm^{-1}]	1.859	1.714
F(000)	1092.0	1196.0
Crystal Size (mm)	0.135 × 0.111 × 0.099	0.864 × 0.292 × 0.138
2θ range for data collection	8.856 to 145.034	8.884 to 145.224
Reflections collected	9080	23142
Independent reflections	4375	4989
R(int)	0.0873	0.0275
Data / restraints / parameters	4375 / 21 / 316	4989 / 0 / 352
Goof (F^2)	1.034	1.072
R_I [I>2σ(I)]	0.0928	0.0650
wR_2 [all data]	0.2632	0.1527
Max/min res. e density [eÅ^{-3}]	1.53 and -1.38	1.01 and -1.39

Table S6. Selected bond lengths [Å] for **1** [Cu^{II}**L**^{Et}](BF_4) reported previously, in Ref [7].

Bond Length [Å]		**Bond Angle [◦]**	
Cu(1)-N(1)	1.932(5)	N(2)-Cu(1)-N(1)	96.4(2)
Cu(1)-(N2)	1.898(6)	N(2)-Cu(1)-N(4)	166.2(2)
Cu(1)-N(4)	1.932(6)	N(1)-Cu(1)-N(4)	96.1(2)
Cu(1)-N(3)	2.036(6)	N(2)-Cu(1)-N(3)	83.6(2)
		N(4)-Cu(1)-N(3)	84.0(2)
		N(1)-Cu(1)-N(3)	179.3(3)

Table S7. Selected bond lengths [Å] for **2** [Cu^{II}**L**$^{Et\text{-}MePy}$](BF_4)**.**

Bond Length [Å]		**Bond Angle [◦]**	
Cu(1)-N(1)	1.940(6)	N(2)-Cu(1)-N(1)	94.7(3)
Cu(1)-(N2)	1.944(7)	N(2)-Cu(1)-N(4)	157.9(3)
Cu(1)-N(4)	1.939(4)	N(1)-Cu(1)-N(4)	94.9(1)
Cu(1)-N(3)	2.106(5)	N(2)-Cu(1)-N(3)	83.5(2)
Cu(1)-N(5)	2.247(6)	N(4)-Cu(1)-N(3)	85.1(3)
		N(1)-Cu(1)-N(3)	174.4(3)
		N(5)-Cu(1)-N(4)	92.0(3)
		N(3)-Cu(1)-N(5)	81.0(2)
		N(1)-Cu(1)-N(5)	104.6(2)
		N(2)-Cu(1)-N(5)	104.9(2)

Table S8. Selected bond lengths [Å] for **3** [Cu^{II}**L**^{EtPy2}](BF_4).

Bond Length [Å]		**Bond Angle [◦]**	
Cu(1)-N(1)	1.975(3)	N(2)-Cu(1)-N(1)	89.1(1)
Cu(1)-(N2)	1.992(3)	N(2)-Cu(1)-N(4)	178.4(2)
Cu(1)-N(4)	1.984(3)	N(1)-Cu(1)-N(4)	89.4(1)
Cu(1)-N(3)	2.206(3)	N(2)-Cu(1)-N(3)	90.3(1)
Cu(1)-N(5)	2.173(3)	N(4)-Cu(1)-N(3)	90.7(1)
		N(1)-Cu(1)-N(3)	123.9(1)
		N(5)-Cu(1)-N(4)	90.5(1)
		N(3)-Cu(1)-N(5)	107.7(1)
		N(1)-Cu(1)-N(5)	128.4(2)
		N(2)-Cu(1)-N(5)	90.7(1)

4. NMR Spectra

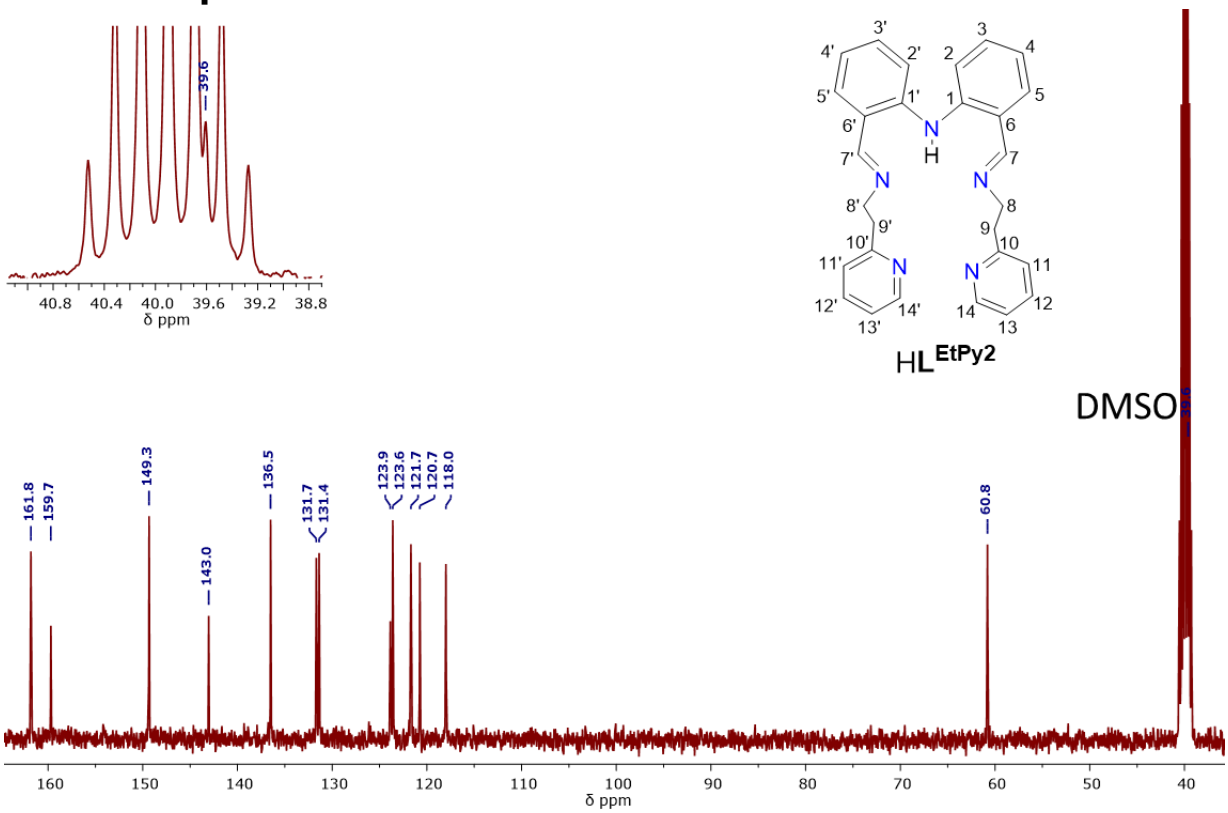

Figure S35. ^{13}C-NMR spectrum of N5-noncyclic ligand HL^{EtPy2} (400 MHz, d_6-DMSO, 298 K): δ (ppm) = 161.81 (C_{14}), 159.71(C_{10}), 149.34 (C_7), 143.04 (C_1), 136.51 (C_4), 131.68 (C_{11}), 131.38 (C_{13}), 123.87 (C_6), 123.60 (C_2), 121.68 (C_5), 120.74 (C_{12}), 117.99 (C_3), 60.80 (C_8), 39.61(C_9).

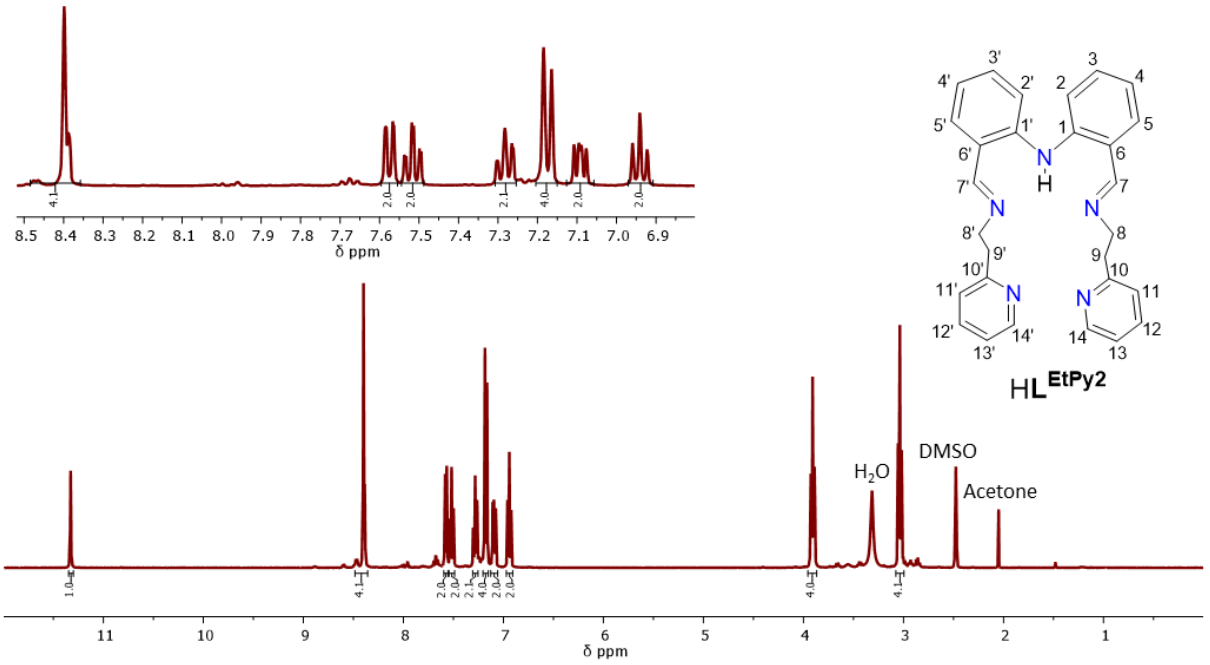

Figure S36. H-nmr spectrum of N5-noncyclic ligand H**L**^{EtPy2} (400 MHz, DMSO-d_6): δ (ppm) = 11.33 (s, 1H, NH), 8.39 (dt, J = 4.3, 1.2 Hz, 4H, $H_{7,7'}$ and $H_{14,14'}$), 7.57 (dd, J = 7.7, 1.6 Hz, 2H, $H_{11,11'}$), 7.52 (td, J = 7.6, 1.9 Hz, 2H, $H_{5,5'}$), 7.28 (ddd, J = 8.6, 7.1, 1.6 Hz, 2H, $H_{13,13'}$), 7.20 – 7.15 (m, 4H, $H_{3,3'}$ and $H_{2,2'}$), 7.09 (ddd, J = 7.6, 4.8, 1.2 Hz, 2H, $H_{4,4'}$), 6.94 (td, J = 7.4, 1.1 Hz, 2H, $H_{12,12'}$), 3.91 (td, J = 7.2, 1.2 Hz, 4H, $H_{8,8'}$), 3.04 (t, J = 7.2 Hz, 4H, $H_{9,9'}$).

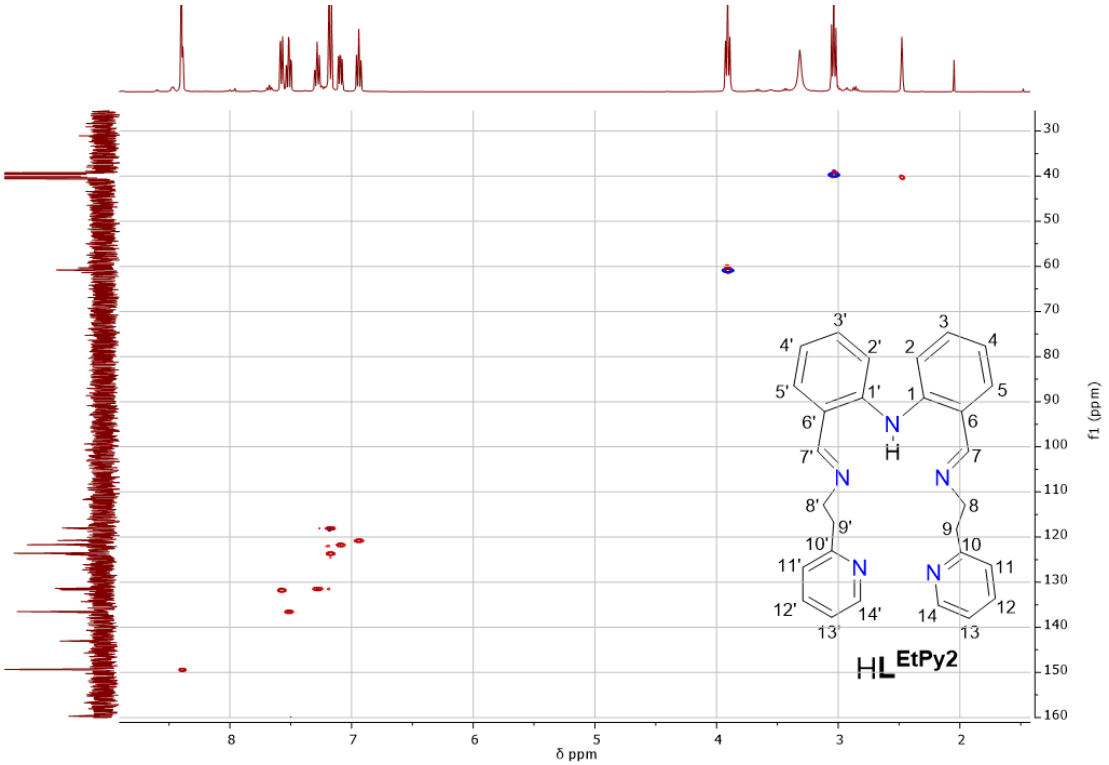

Figure S37. HSQC nmr spectrum of N5-noncyclic ligand H**L**^{EtPy2}. Note that the aliphatic proton at δ = 3.91 ppm is bonded to the C8 δ = 39.6 ppm masked by DMSO signal.

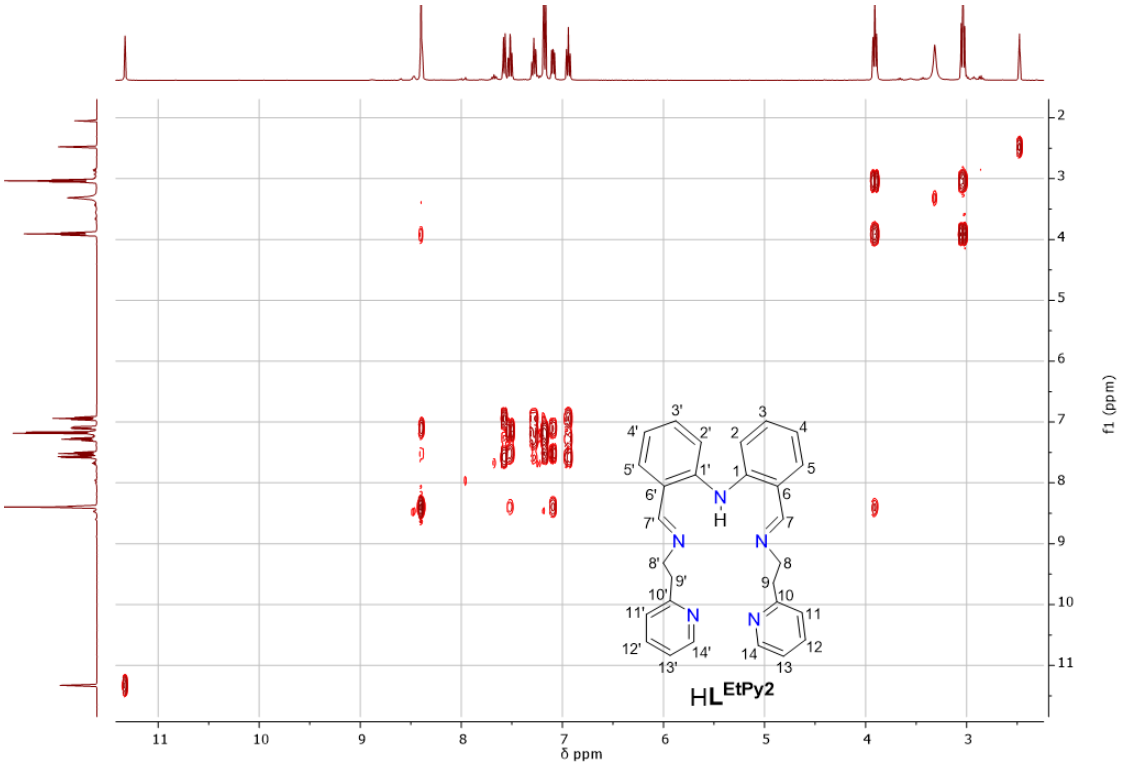

Figure S38. **H**-COSY-nmr spectrum of N5-noncyclic ligand H**L**^{EtPy2}.

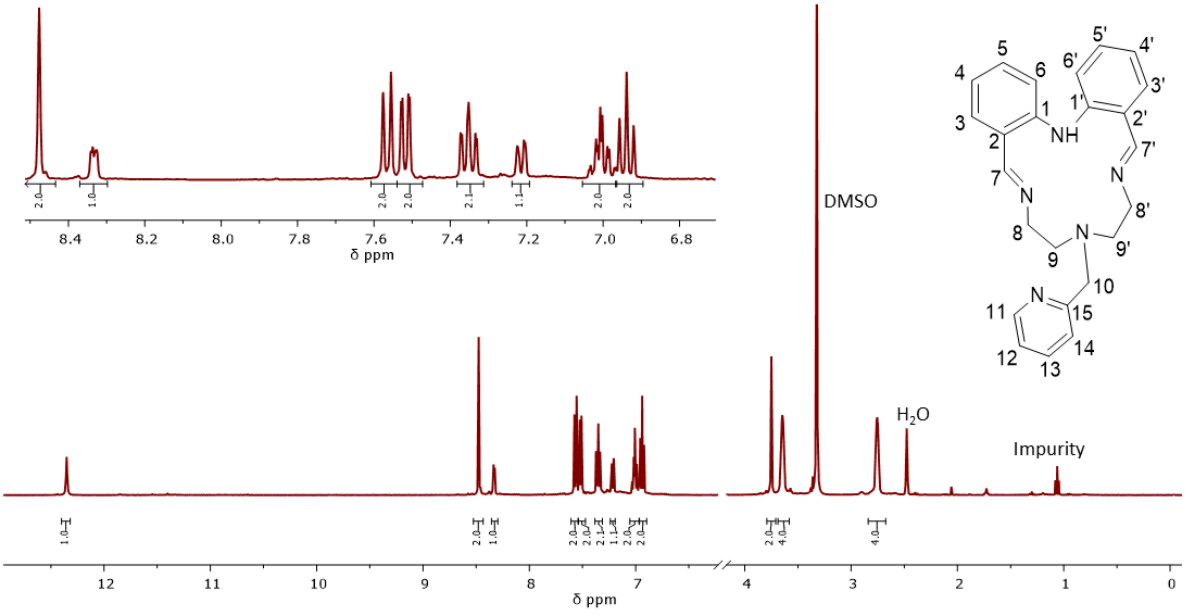

Figure S39. **H**-nmr spectrum of N5-macrocyclic ligand H**L**$^{Et\text{-}MePy}$ (400 MHz, DMSO-d_6): δ (ppm) = 12.35 (s, 1H, NH), 8.48 (s, 2H, H_7), 8.36 – 8.30 (m, 1H, H_{11}) 7.57 (dd, J = 8.4, 1.1 Hz, 2H, H_6), 7.52 (dd, J = 7.7, 1.7 Hz, 2H, H_3), 7.35 (ddd, J = 8.5, 7.2, 1.7 Hz, 2H, H_5), 7.21 (dt, J = 7.1, 1.1 Hz, H_{13}), 7.05 – 6.97 (m, 2H, H_{12}, H_{14}), 6.94 (td, J = 7.4, 1.0 Hz, 2H, H_4), 3.75 (s, 2H, H_{10}), 3.65 (m, 4H, H_8), 2.81 – 2.68 (m, 4H, H_9)

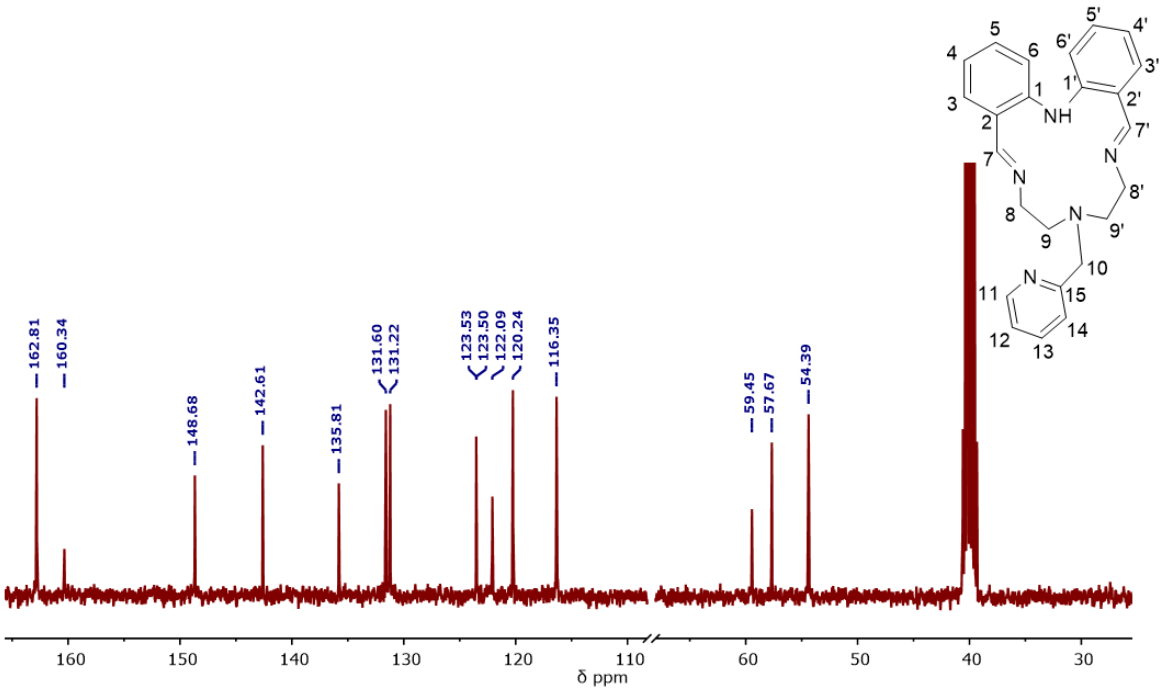

Figure S40. ^{13}C-NMR spectrum of N5-macrocyclic ligand HL$^{Et\text{-}Py}$ (400 MHz, DMSO-d_6, 298 K): δ (ppm) = 162.81 (C_7), 160.34 (C_{15}), 148.68 (C_{11}), 142.61 (C_1), 135.81 (C_{13}), 131.60 (C_3), 131.21 (C_5), 123.53 (C_2), 123.50 (C_{14}), 122.09 (C_{12}), 120.24 (C_4), 116.35 (C_6), 59.45 (C_{10}), 57.67 (C_{9v}, 54.39 (C_8).

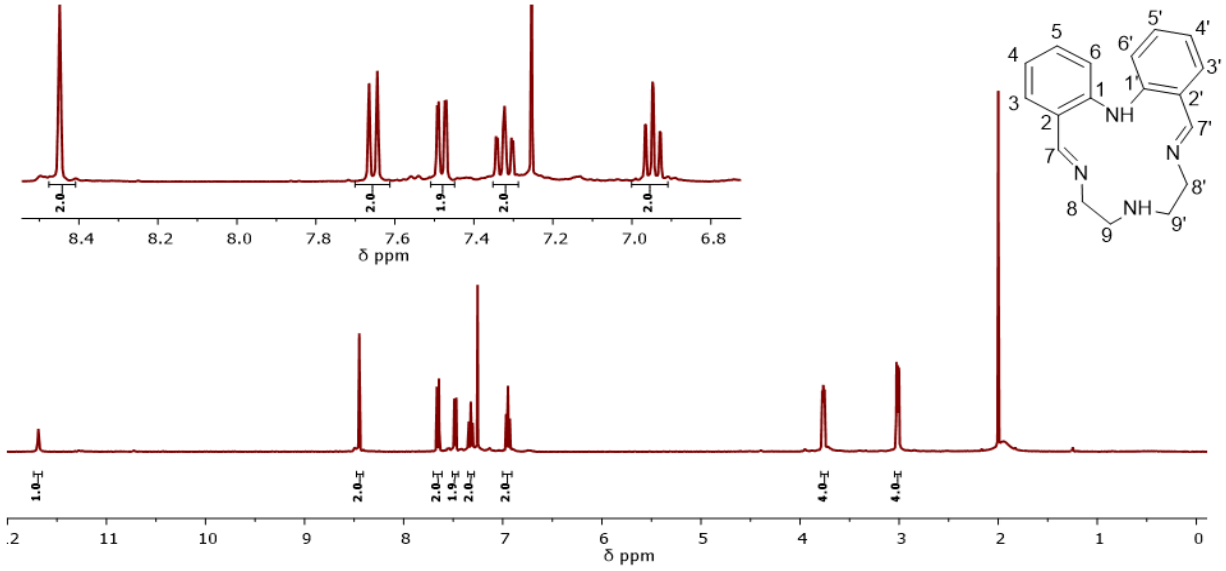

Figure S41. ^{1}H-NMR spectrum of N4-macrocyclic ligand H**L**^{Et} in $CDCl_3$.

5. ESI-MS Spectra of new ligands and complexes

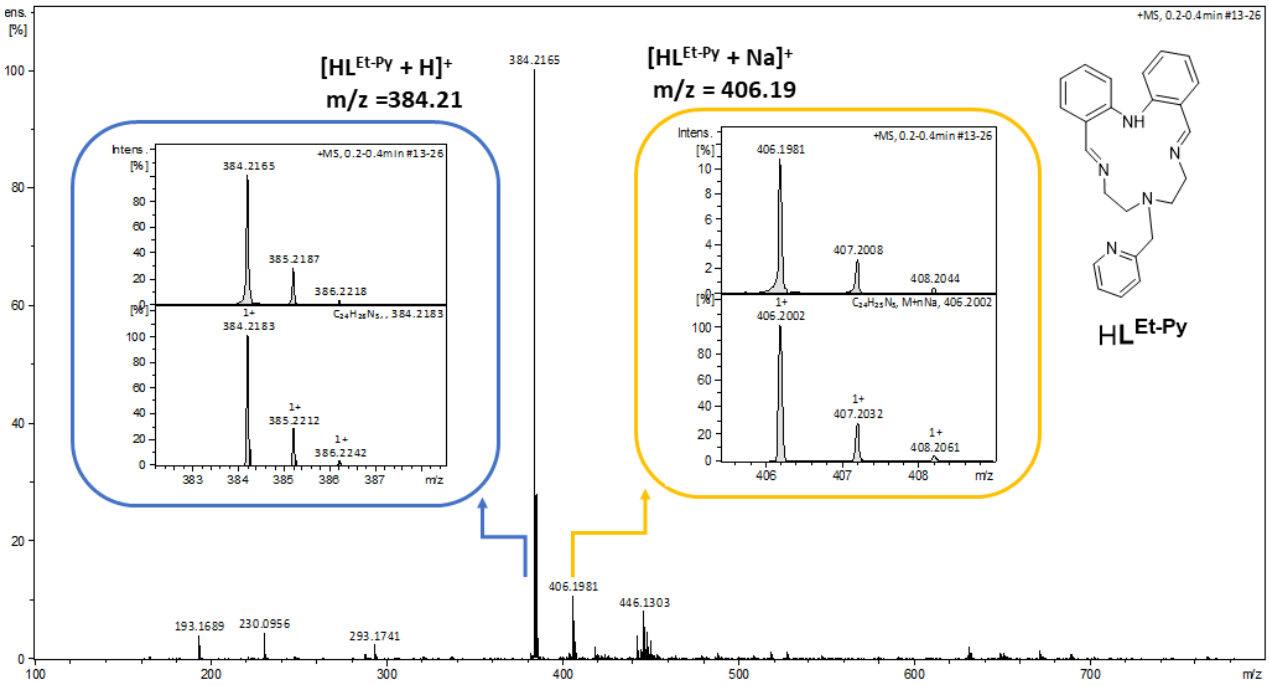

Figure S42. Mass spectrum (MS-ESI-positive mode) of N5-macrocyclic ligand H**L**$^{Et\text{-}Py}$.

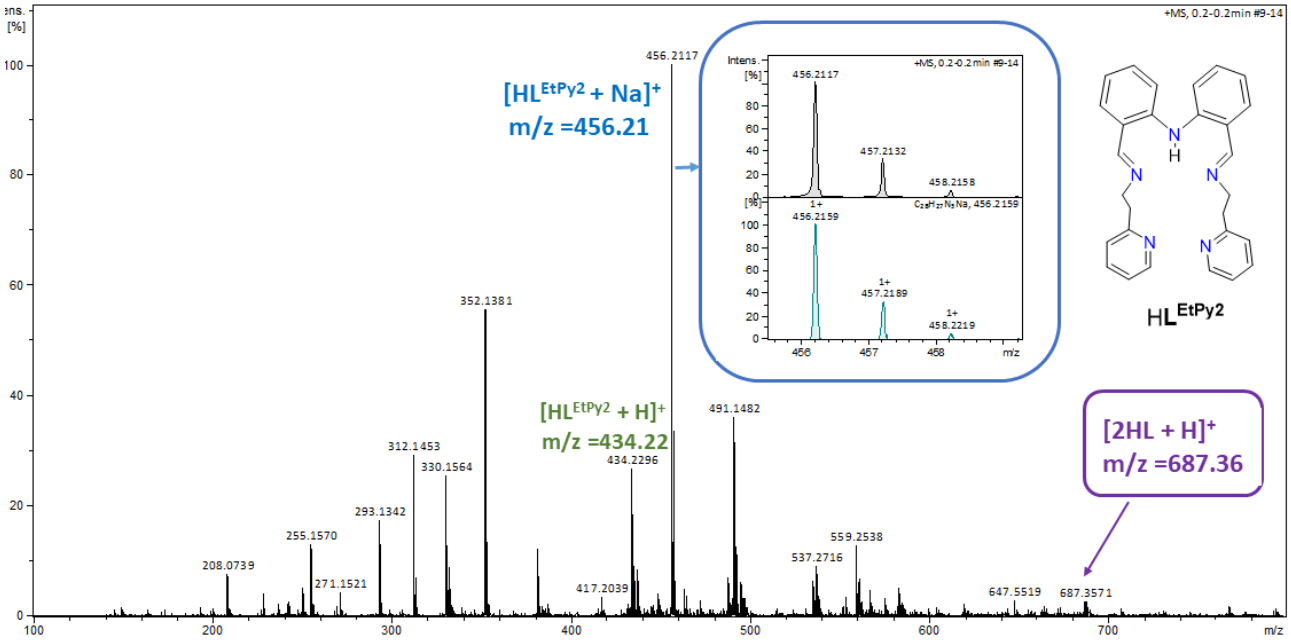

Figure S43. Mass spectrum (MS-ESI-positive mode) of N5-non-cyclic ligand H**L**^{EtPy2}.

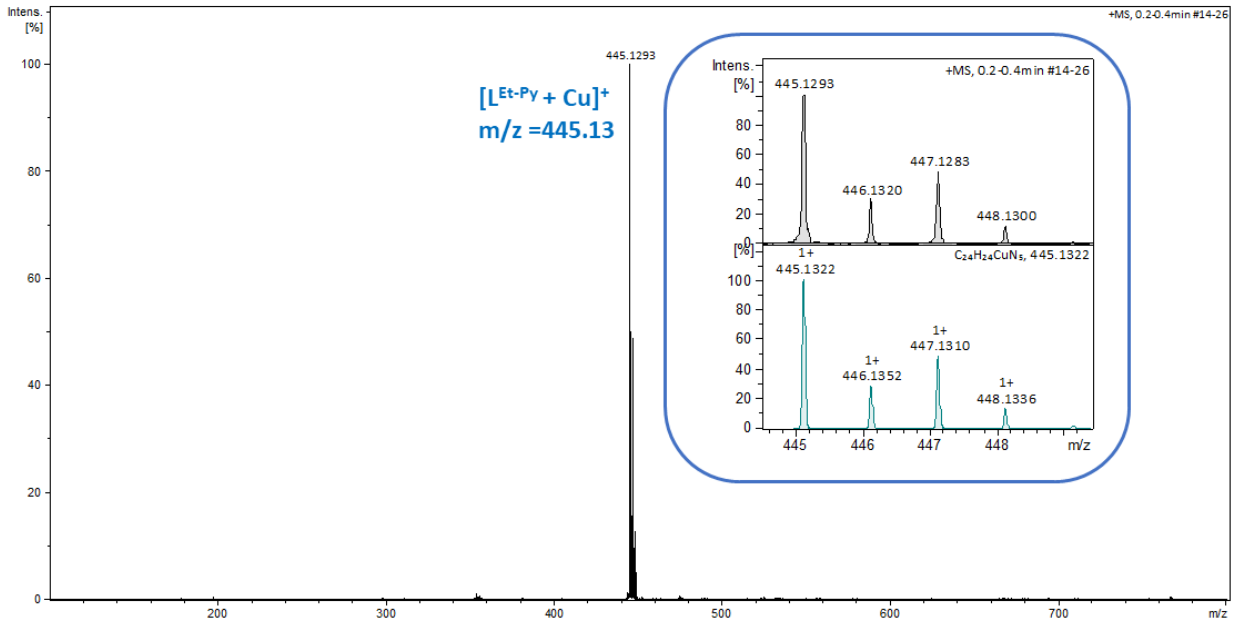

Figure S44. Mass spectrum (MS-ESI-positive mode) of complex **2**, $[Cu^{II}\ \mathbf{L}^{Et\text{-}MePy}]^{+}$.

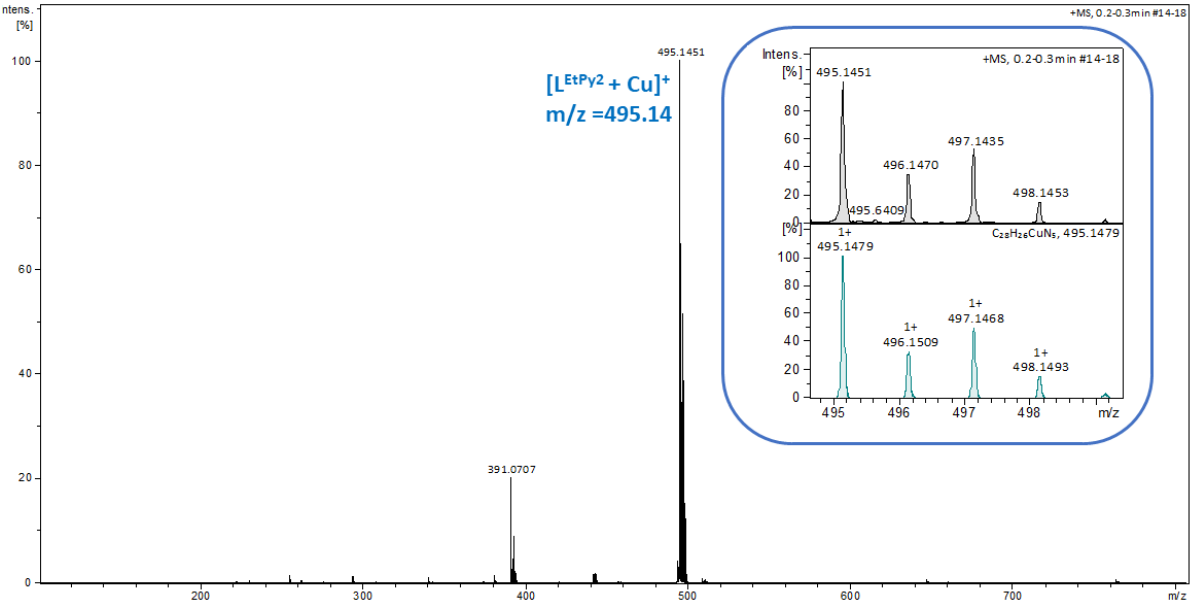

Figure S45. Mass spectrum (MS-ESI-positive mode) of complex **3**, $[Cu^{II}\ \mathbf{L}^{EtPy2}]^{+}$.

6. References

1. M. Kirch, J.-M. Lehn and J.-P. Sauvage, 'Hydrogen Generation by Visible Light Irradiation of Aqueous Solutions of Metal Complexes. An approach to the photochemical conversion and storage of solar energy', *Helv. Chim. Acta*, **1979**, *62*, 1345-1384.
2. J.-M. Lehn and R. Ziessel, 'Photochemical generation of carbon monoxide and hydrogen by reduction of carbon dioxide and water under visible light irradiation', *PNAS*, **1982**, *79*, 701-704.
3. R. W. Hogue, O. Schott, G. S. Hanan and S. Brooker, 'A smorgasboard of 17 cobalt complexes active for photocatalytic hydrogen evolution', *Chem. Eur. J.*, **2018**, *24*, 9820-9832.
4. B. Probst, C. Kolano, P. Hamm and R. Alberto, 'An Efficient Homogeneous Intermolecular Rhenium-Based Photocatalytic System for the Production of H2', *Inorg. Chem.*, **2009**, *48*, 1836-1843.
5. J. Hawecker, J. M. Lehn and R. Ziessel, 'Efficient homogeneous photochemical hydrogen generation and water reduction mediated by cobaloxime or macrocyclic cobalt complexes', *NJC*, **1983**, *7*, 271-277.
6. P. Zanello, *Inorganic Electrochemistry: Theory, Practice and Application*, Royal Society of Chemistry, Cambridge, UK, 2003.
7. R. Sanyal, S. A. Cameron and S. Brooker, 'Synthesis and complexes of an N_4 Schiff-base macrocycle derived from 2,2'-iminobisbenzaldehyde', *Dalton Trans.*, **2011**, *40*, 12277-12287.
8. R. K. Wilson and S. Brooker, 'Oxidative dehydrogenation of a new tetra-amine N_4–donor macrocycle tunes the nickel(II) spin state from high spin to low spin', *Dalton Trans.*, **2013**, *42*, 12075-12078.
9. D. S. C. Black and N. E. Rothnie, 'Metal template reactions. XIX. Macrocyclic metal complexes derived from 2,2'-iminobisbenzaldehyde and some primary diamines with additional nitrogen donor atoms', *Aust. J. Chem.*, **1983**, *36*, 2395-2406; E. D. Bergmann, M. Rabinovitz and I. Agranat, *Bull. Res. Counc. Isr. Sect. A: Chem.*, **1962**, *11*, 149; S. A. Cameron and S. Brooker, 'Metal-free and dicopper(II) complexes of Schiff base [2+2] macrocycles derived from 2,2'-iminobisbenzaldehyde: syntheses, structures and electrochemistry', *Inorg. Chem.*, **2011**, *50*, 3697-3706.
10. *CrysAlisPro*, CrysAlisPro, Version 171.37.33; Agilent Technologies: Yarnton, Oxfordshire, **2014**.
11. G. Sheldrick, 'Crystal structure refinement with SHELXL', *Acta Crystallogr., Sect. C*, **2015**, *71*, 3-8.
12. O. V. Dolomanov, L. J. Bourhis, R. J. Gildea, J. A. K. Howard and H. Puschmann, 'OLEX2: a complete structure solution, refinement and analysis program', *J. Appl. Cryst.*, **2009**, *42*, 339-341.
13. C. F. Macrae, I. J. Bruno, J. A. Chisholm, P. R. Edgington, P. McCabe, E. Pidcock, L. Rodriguez-Monge, R. Taylor, J. van de Streek and P. A. Wood, 'Mercury CSD 2.0 - new features for the visualization and investigation of crystal structures', *J. Appl. Crystallogr.*, **2008**, *41*, 466-470.
14. S. K. Das and J. Frey, 'Regioselective double Boekelheide reaction: first synthesis of 3,6-dialkylpyrazine-2,5-dicarboxaldehydes from dl-alanine', *Tetrahedron Lett.*, **2012**, *53*, 3869-3872.